A CASE STUDY OF THE NEWCASTLE GEOTHERMAL SYSTEM, IRON COUNTY, UTAH

by

Robert E. Blackett and Michael A. Shubat

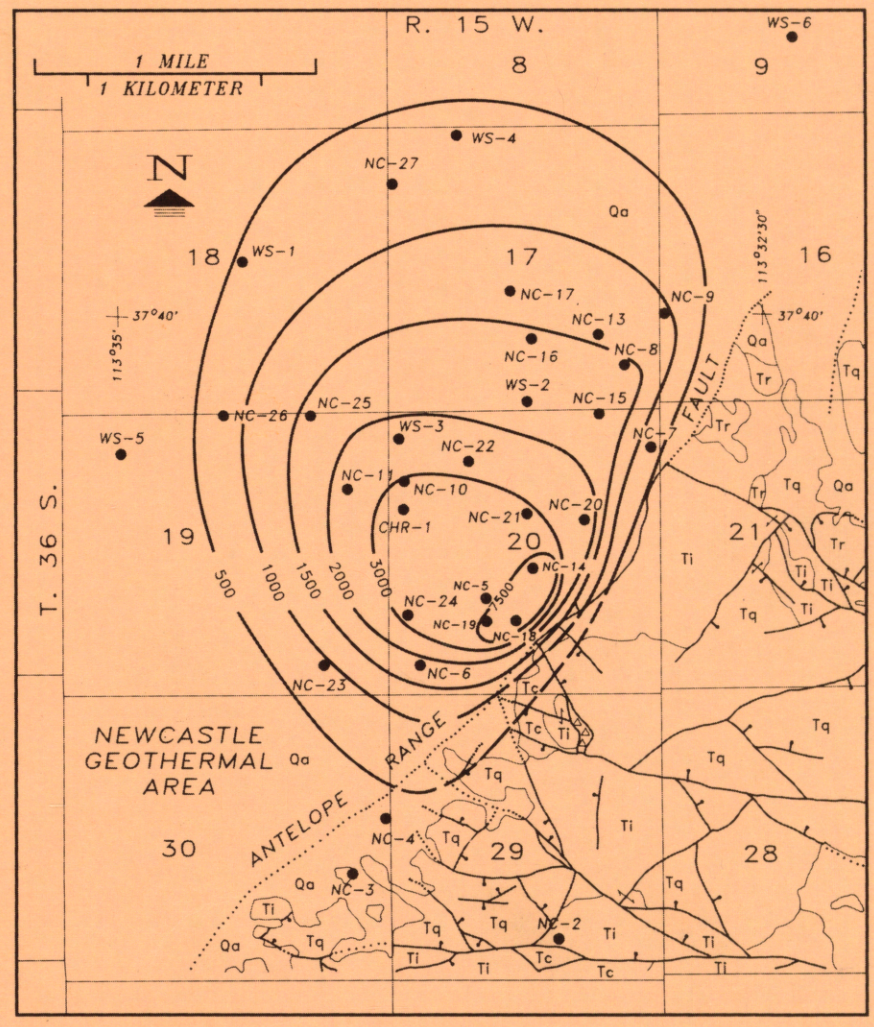

SPECIAL STUDY 81 1992

UTAH GEOLOGICAL SURVEY

a division of

UTAH DEPARTMENT OF NATURAL RESOURCES

UTAH GEOLOGICAL SURVEY
2363 South Foothill Drive
Salt Lake City, Utah 84109-1491

THE UTAH GEOLOGICAL SURVEY is organized into three geologic programs with Administration, Editorial, and Computer Resources providing necessary support to the programs. THE ECONOMIC GEOLOGY PROGRAM undertakes studies to identify coal, geothermal, uranium, hydrocarbon, and industrial and metallic mineral resources; to initiate detailed studies of the above resources including mining district and field studies; to develop computerized resource data bases, to answer state, federal, and industry requests for information; and to encourage the prudent development of Utah's geologic resources. The APPLIED GEOLOGY PROGRAM responds to requests from local and state governmental entities for engineering geologic investigations; and identifies, documents, and interprets Utah's geologic hazards. The GEOLOGIC MAPPING PROGRAM maps the bedrock and surficial geology of the state at a regional scale by county and at a more detailed scale by quadrangle. Information Geologists answer inquiries from the public and provide information about Utah's geology in a non-technical format.

The UGS manages a library which is open to the public and contains many reference works on Utah geology and many unpublished documents on aspects of Utah geology by UGS staff and others. The UGS has begun several computer data bases with information on mineral and energy resources, geologic hazards, stratigraphic sections, and bibliographic references. Most files may be viewed by using the UGS Library. The UGS also manages a sample library which contains core, cuttings, and soil samples from mineral and petroleum drill holes and engineering geology investigations. Samples may be viewed at the Sample Library or requested as a loan for outside study.

The UGS publishes the results of its investigations in the form of maps, reports, and compilations of data that are accessible to the public. For information on UGS publications, contact the UGS Sales Office, 2363 South Foothill Drive, Salt Lake City, Utah 84109-1491, (801) 467-7970.

A CASE STUDY OF THE NEWCASTLE GEOTHERMAL SYSTEM, IRON COUNTY, UTAH

by
Robert E. Blackett and Michael A. Shubat

SPECIAL STUDY 81 **1992**
UTAH GEOLOGICAL SURVEY
a division of
UTAH DEPARTMENT OF NATURAL RESOURCES

DISCLAIMER

This report summarizes work supported in part by the U.S. Department of Energy (grant number DE-FG07-88ID12756). *The U.S. Department of Energy or its employees makes no warranty, express or implied, or assumes any legal liability or responsibility for the accuracy, completeness, or usefulness of any information, apparatus, product, or process disclosed, or represents that its use would not infringe privately owned rights. Reference to any specific commercial product, process, or service by trade name, trademark, manufacturer, or otherwise, does not necessarily constitute or imply its endorsement, recommendation, or favoring by the U.S. Department of Energy, or any of their agencies.*

CONTENTS

FIGURES

TABLES

PLATES (in pocket)

A CASE STUDY OF THE NEWCASTLE GEOTHERMAL SYSTEM, IRON COUNTY, UTAH

by
Robert E. Blackett and Michael A. Shubat
Utah Geological Survey

ABSTRACT

The Utah Geological Survey, in cooperation with University of Utah and the University of Utah Research Institute, conducted geological, geophysical, and geochemical studies over the concealed, moderate-temperature, Newcastle geothermal system located in southwestern Utah. Temperature-depth measurements from 25 thermal-gradient drill holes and three geothermal production wells define a thermal anomaly, centered near the surface trace of the range-bounding Antelope Range fault, and an elongate thermal plume extending northward and westward within a shallow aquifer. The thermal aquifer generally occurs at depths from 65 to 95 meters (210 to 310 ft). A temperature of 130°C (266°F), measured in the out-flow plume of the system, is the highest temperature recorded to date. Higher temperatures, however, are expected in the fluid upflow zone. The new heat-flow data yielded a computed, anomalous heat loss of 12.4 megawatts (thermal). Chemical analyses of water samples indicate that thermal fluid, produced from wells penetrating the outflow plume, is a mixture of meteoric water likely derived from recharge areas in the Pine Valley Mountains and cold, shallow ground water. Detailed self-potential (SP) and resistivity surveys define the geometry of the probable upflow zone indicating that the thermal fluid issues from a short segment of the Antelope Range fault and discharges laterally into a shallow aquifer beneath the Escalante Desert. Self-potential data show a high-amplitude, elliptical SP minimum coincident with the center of the thermal anomaly and with the subsurface intersection of the Antelope Range fault with older faults. We postulate that this SP minimum marks the primary upflow conduit of the hydrothermal system where most of the thermal fluid discharges from transmissive structures. Additional leakage of thermal fluid, as shown by resistivity data, occurs over a minimum distance of 1.5 kilometers (1 mi) along the trace of the Antelope Range fault.

INTRODUCTION

Location and Background

Although many hydrothermal-geothermal systems are known in the Basin and Range Province of the western United States, Brook and others (1979, p. 35) believe that undiscovered resources constitute about four-fifths of the total accessible hydrothermal resource base. They suggest that these undiscovered resources consist of extensions of known hydrothermal systems and isolated, concealed hydrothermal systems. Concealed hydrothermal systems have no surface expression of hydrothermal activity. The ability to detect such concealed hydrothermal systems is, therefore, important to continued geothermal exploration and development. This report documents a study of a hidden or concealed hydrothermal system at Newcastle, Utah.

Newcastle is a rural farming community situated in southwestern Utah. In 1975 during test pumping of a newly drilled irrigation well, the Christensen Brothers — a farming cooperative — accidentally discovered a concealed hydrothermal system. Temperature profiles from the well revealed a hot-water aquifer with a maximum temperature of 108°C (226°F) between depths of 85 and 95 meters (279 and 312 ft) (Rush, 1983, p. 19). This was the first recorded encounter with the geothermal system at Newcastle although early settlers reportedly abandoned hand digging of a water well because of excessive heat (Boyd Christensen, personal communication, 1988).

The community of Newcastle lies along the southeast edge of the Escalante Desert about 48 kilometers (30 mi) west of Cedar City, along Utah State Route 56 (figure 1). Cedar City is roughly 440 kilometers (275 mi) southwest of Salt Lake City via Interstate 15. The communities of Enterprise and St. George, Utah are about 13 kilometers (8 mi) southwest and 64 kilometers (40 mi) to the south of Newcastle, respectively. Developed geothermal areas within the region include the Roosevelt Hot Springs Known Geothermal

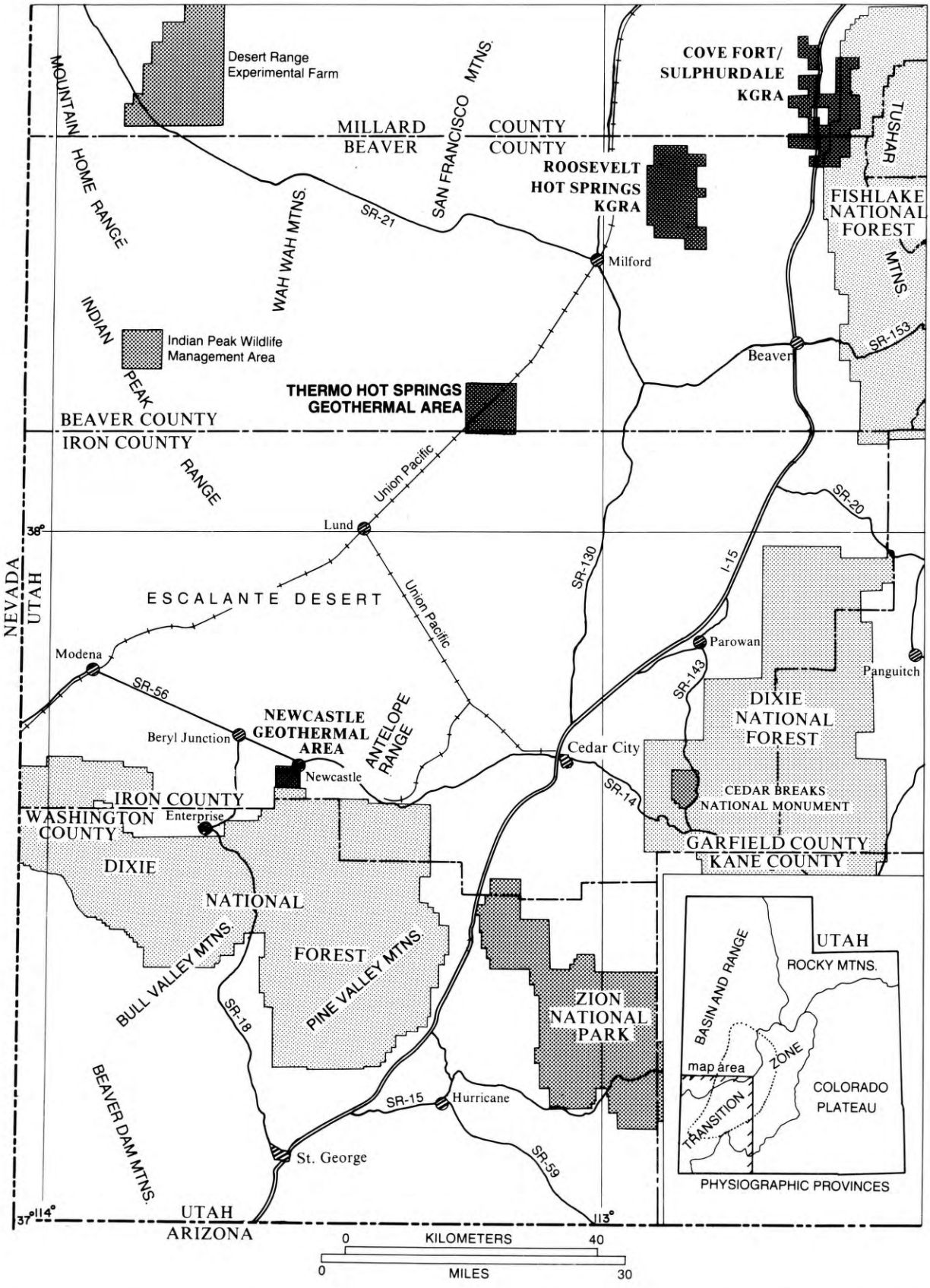

Figure 1. General location map with respect to communities, highways, railroads, geographic features, other geothermal areas, and principal administrative boundaries in southwest Utah. Dotted line on inset map indicates the approximate outline of the Sevier thermal area defined by Mabey and Budding (1987).

Resource Area (KGRA), and the Cove Fort—Sulphurdale KGRA, located roughly 105 kilometers (65 mi), and 120 kilometers (75 mi) to the northeast, respectively. Utah Power and Light Company operates a 26 megawatt (MW) geothermal power plant at Roosevelt, and the Utah Municipal Power Authority operates a 13.5 MW geothermal power plant at Cove Fort.

Previous Work

Since Christensen Brothers drilled the discovery well, several organizations and individuals have studied the geothermal system. Denton (1976) conducted a helium survey across the area and detected a broad helium anomaly around the discovery well and along the nearby range front. Rush (1977) reported the results of temperature-gradient measurements for the Newcastle area and the Escalante Desert as well as for other areas in Utah. Pe and Cook (1980) conducted a gravity survey in the region and interpreted a large, northeast-oriented gravity low centered northwest of Newcastle as a deep graben.

Chapman and others (1981), using temperature-gradient data obtained from various sources, calculated a thermal power loss of 13 megawatts from an area of 9.4 square kilometers (3.6 mi^2), assuming a water temperature of 110°C (230°F) and a discharge rate of 32 liters/second (507 gal/min). Rush (1983) reported the results of chemical analysis of a sample of the Newcastle thermal water and estimated a reservoir temperature of 140°C to 170°C (284°F to 338°F) based upon chemical geothermometry. Rush (1983) also presented a temperature profile of the Christensen Brothers' discovery well, a potentiometric map, and a preliminary heat-flow map of the Newcastle area. Hoover and Pierce (1987) reported the results of eight audio-magnetotelluric soundings in the Newcastle area, with the lowest resistivity values measured at a station east of the Christensen Brothers' discovery well. Mabey and Budding (1987) compiled available data on the Newcastle system and presented a geothermal model suggesting that hot water rises along a fault zone near the base of the hills southeast of Newcastle and discharges into an aquifer in unconsolidated Quaternary sediments.

Purpose and Scope

Past exploration in low- and moderate-temperature systems of the Great Basin shows that the relatively small area associated with fluid upflow and elevated temperatures is often difficult to detect by drilling widely spaced temperature-gradient holes or by other methods. By studying the Newcastle geothermal system, we hoped to develop a basic understanding of the concealed hydrothermal system as a tool for assessing other geothermal areas of the Great Basin. The emphasis of our work centered on determining (1) the distribution of subsurface heat and the movement of thermal fluid, (2) the location and geometry of bedrock structures that might control fluid movements, (3) the chemical character of the geothermal water, and (4) the geometry of the bedrock beneath the Escalante Desert.

Field studies included: (1) drilling and monitoring temperatures in shallow thermal-gradient boreholes, (2) mapping geologic units and performing structural studies in the adjacent mountains, (3) conducting detailed gravity surveys, (4) conducting electrical resistivity and self-potential (SP) surveys, (5) collecting water samples for determining major ions and light stable isotope analyses, and (6) mapping Quaternary units.

Physiography, Climate, and Hydrology

The Newcastle geothermal area lies within the 50 to 130 kilometers (30 to 80 miles) wide Transition Zone, a northeast-southwest-trending belt in southwest and south-central Utah (figure 1). The zone contains geologic and geomorphic features typical of both the Basin and Range Province, to the west, and the Colorado Plateau Province to the east. Landforms within this zone include flat-topped plateaus and sharp-crested ranges separated by alluvial valleys. Horsts and grabens, resulting from the formation of long, Cenozoic extensional faults, are common.

The Escalante Desert, an elliptical basin occupying an area roughly 70 by 45 kilometers (45 by 28 mi), is surrounded by the Pine Valley Mountains to the southeast, the Bull Valley Mountains to the southwest, the Antelope Range to the east, and the Wah Wah Mountains and Indian Peak Range to the northwest. It is a high desert, lying at elevations generally between 1,547 and 1,676 meters (5,075 and 5,500 ft) above sea level, and receiving typically less than 30.5 cm (12 in) of precipitation annually (Mower and Sandberg, 1982, p. 5). Surrounding mountains lie at elevations usually less than 2,440 meters (8,000 ft), although peaks in the Indian Peak Range and the Pine

Valley Mountains exceed 2,743 meters (9,000 ft). Annual precipitation in the Pine Valley Mountains often exceeds 50 cm (20 in). Mild summers and cool winters are typical of this region where daytime summer temperatures seldom exceed 38°C (100°F) and where nighttime winter temperatures seldom fall below -25°C (-13°F) (Mower and Sandberg, 1982, p. 8).

Surface hydrology of the Escalante Desert drainage area consists of three perennial streams issuing from the Pine Valley and Bull Valley Mountains — Pinto Creek near Newcastle, Little Pine Creek near Enterprise, and Mountain Meadow Creek located between the two towns — and a number of intermittent and ephemeral streams that enter the valley from the surrounding ranges (Mower and Sandberg, 1982, p. 12). Water from perennial streams is completely used for irrigation. Intermittent and ephemeral streams infiltrate into unconsolidated deposits and disappear shortly after issuing onto the valley floor. Some of the larger intermittent and ephemeral streams flow for several kilometers before infiltrating and disappearing within the valley floor. Surface water that doesn't infiltrate is lost through evapotranspiration. No streams exit the Escalante Desert.

GEOLOGY

Regional Geology

Mabey and Budding (1987) proposed the name "Sevier thermal area" for a large region of southwestern Utah characterized by relatively high heat flow, abundant young igneous rocks, and numerous late-Cenozoic normal faults. There are seven known high- and moderate-temperature geothermal systems within the Sevier thermal area. These systems occur in or along the margins of intermontane valleys in the eastern part of the Basin and Range geologic province, or the central portion of the Transition Zone (figure 1). Compared to a continental average of roughly 50 milliwatts per square meter (mW/m^2), heat flow in the Sevier thermal area averages 88 mW/m^2 (Mabey and Budding, 1987, p. 9). The Intermountain seismic belt, a zone of high earthquake activity identified by Smith and Sbar (1974) that runs generally north-south through central Utah, changes orientation from north to southwest within the Sevier thermal area. Abundant Oligocene and Miocene volcanic and intrusive rocks occur in the southern part of the Sevier thermal area, while Pliocene to Quaternary age basalt and young silicic rocks occur in the northern part.

High regional heat flow coupled with complex geologic structure and an ample supply of meteoric fluids from recharge areas such as the Pine Valley and Tushar Mountains creates conditions favorable for the development of hydrothermal convection systems. Young igneous bodies may also supply heat to some of the geothermal systems in the Sevier thermal area.

The Newcastle geothermal area lies along the southern margin of the Escalante Desert, an elliptical depression measuring approximately 70 x 45 kilometers (44 x 28 mi) surrounded by mountains and hills composed primarily of Tertiary ash-flow tuffs, flows and domes. Ash-flow tuff units range in age from 32 to 19 million years. Rhyolite and dacite flows and domes range in age from 13 to 8.5 million years.

Klauk and Gourley (1983, p. 3) describe four significant geologic events for the Escalante Desert: (1) large-scale thrust faulting of the Cretaceous Sevier orogeny, (2) mid-Tertiary igneous activity confined to broad, east-west-oriented belts, (3) late Tertiary and Quaternary (basin and range) extensional tec-

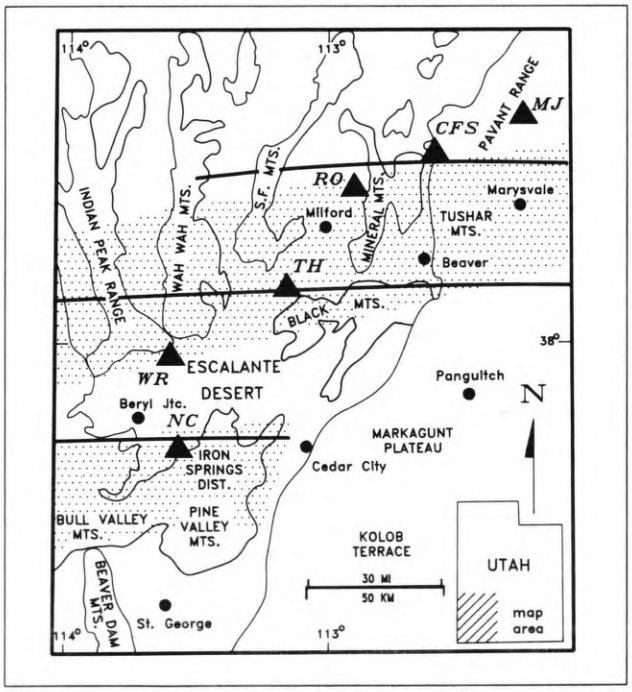

Figure 2. Location of the Newcastle (NC) study area with respect to Thermo Hot Springs (TH), Roosevelt Hot Springs (RO), Cove Fort-Sulphurdale (CFS), Wood Ranch (WR), and Monroe-Joseph (MJ) geothermal systems (triangles) of the Sevier thermal area. East-west heavy solid lines denote (from north to south) the Black Rock, Blue Ribbon, and Timpahute lineaments. Stipple pattern denotes the Pioche-Marysvale and the Delamar-Iron Springs mineralligneous belts to the north and south, respectively (after Rowley and others, 1979).

tonism that produced numerous north-south-oriented fault-block mountains, and (4) periods of late-Tertiary and Quaternary volcanism with some associated intrusive activity. Sevier-age thrust faults have been mapped near the Escalante Desert, and evidence of Paleozoic strata thrust upon Jurassic strata is present in at least one deep, oil and gas exploratory well drilled in the Escalante Desert (Shubat and McIntosh, 1988, p.6). The valley is situated between two major, roughly east-west-oriented mineral, or igneous, belts. The Pioche-Marysvale mineral belt lies to the north, and the Delamar-Iron Springs mineral belt lies to the south (figure 2). Rowley and others (1979) suggest that the Pioche-Marysvale and the Delamar-Iron Springs igneous belts are structurally controlled, and associated with two east-west-oriented lineaments — the Blue Ribbon lineament to the north and the Timpahute lineament to the south.

Stratigraphy

Exposed bedrock units at Newcastle, described in detail by Siders and others (1990), and shown on plate 1, range in age from Upper Cretaceous to upper Miocene (plate 2). These units consist of older sedimentary rocks overlain by a series of middle-Tertiary ash-flow tuffs of regional extent, and capped by local rhyolite and dacite flows. The oldest unit exposed is the Upper Cretaceous Iron Springs Formation, which consists of light-colored, thin- to thick-bedded sandstone and lesser shale, conglomerate, limestone, and carbonaceous shale. The unit was deposited in braided fluvial and lacustrine environments with sediment derived from the Sevier orogenic highland to the west. The minimum exposed thickness of the Iron Springs is 430 meters (1,400 ft). The Eocene to Oligocene Claron Formation unconformably overlies the Iron Springs Formation and consists of fluvial and lacustrine shale, sandstone, limestone, siltstone, and conglomerate. The unit has a minimum exposed thickness of 130 meters (430 ft) and is about 210 meters (700 ft) thick in nearby areas (Siders and others, 1990).

The Oligocene Isom Formation overlies the Claron Formation. The Isom consists of two densely welded, crystal-poor, ash-flow tuff members of regional extent: the lower Baldhills Tuff Member and upper Hole-in-the-Wall Tuff Member. Both members range in color from dark brown to black and contain sparse phenocrysts of plagioclase, clinopyroxene, and magnetite. Extreme welding produced flattened pumice clasts as much as 0.6 meters (2 ft) in length, and secondary flowage produced stretched vesicles as much as 0.3 meters (1 ft) in length. Intercalated with densely welded tuff near the base of the Baldhills Tuff Member are probable andesitic flows marked by autobrecciation and flow-top scoria, and thin beds of volcanic sandstone. The minimum thickness of the Baldhills Tuff is 330 meters (1,080 ft). The Hole-in-the-Wall Tuff Member consists of a single cooling unit that is about 79 meters (260 ft) thick. The concealed source caldera or vent for the Isom Formation probably lies beneath the Escalante Desert (Best and others, 1989), approximately 35 kilometers (22 mi) northwest of Newcastle. The age of the Isom Formation is approximately 27 million years (Best and others, 1989).

Three regional rhyolitic to andesitic ash-flow tuffs of the Quichapa Group — the Leach Canyon, Bauers, and Harmony Hills units — overlie the Isom Formation and were probably erupted from sources in the Caliente caldera complex, located roughly 65 kilometers (40 mi) west of Newcastle (Williams, 1967). The rhyolitic, moderately welded Leach Canyon Formation, consisting of several cooling units, is approximately 25 million years old (Rowley and others, 1979), and contains 20 to 30 percent phenocrysts of plagioclase, quartz, sanidine, and biotite and reddish lithic fragments. It is about 177 meters (580 ft) thick near Newcastle. The Bauers Tuff Member of the Condor Canyon Formation is rhyolitic, crystal-poor, densely welded, approximately 23 million years old (Rowley and others, 1979), and about 130 meters (430 ft) thick. The tuff contains phenocrysts of plagioclase, sanidine, and bronze biotite and abundant highly flattened pumice clasts. The Bauers Tuff erupted from the Clover Creek caldera located in Lincoln County, Nevada (Rowley and Siders, 1988). The Harmony Hills Tuff is a distinctive crystal-rich, andesitic, moderately welded tuff that has a stratigraphic age of about 22.5 million years (personal communication, P. D. Rowley, 1990). It consists of nearly 50 percent crystals of plagioclase, biotite, hornblende, quartz, and pyroxene and is 146 meters (480 ft) thick. An unnamed, laterally extensive volcaniclastic unit, approximately 40 meters (130 ft) thick, overlies the Harmony Hills Tuff and contains abundant clasts and crystal fragments, of Harmony Hills Tuff as well as andesite cobbles. This northward-thickening unit is probably a distal debris-flow

deposit shed from an andesitic highland to the north.

The Racer Canyon Tuff overlies the Quichapa Group rocks and is the youngest regional ash-flow tuff present at Newcastle. The tuff is crystal-rich, rhyolitic, poorly to moderately welded, and greater than 150 meters (490 ft) thick. Southeast of the map area, the Racer Canyon Tuff consists of at least 3 cooling units, and its age is approximately 19 million years (Siders, 1991). An informally named unit, "volcaniclastic rocks of Newcastle Reservoir," overlies the Racer Canyon Tuff and is greater than 300 meters (980 ft) thick. The unit is correlative with the informally named "mine series" of Siders (1985), which has a minimum age of 11.6 million years. The unit consists of intercalated lenses of conglomerate, mudflow breccia, and sandstone, and most clasts are volcanic rocks. Rhyolite and dacite lava flows and domes overlie and intrude the Racer Canyon Tuff in the northeast corner of the map area (plate 1). These informally named units, the "rhyolite of Silver Peak" and "dacite of Bullion Canyon," yielded potassium-argon (K-Ar) ages of 8.4 and 8.5 Ma, respectively (Shubat and Siders, 1988).

A variety of unconsolidated to semi-consolidated deposits overlie the bedrock units and are described in detail by Siders and others (1990). The oldest of the semi-consolidated deposits is upper Miocene to Pliocene in age (labeled Ts on plate 1) and consists of moderately consolidated boulder, cobble, and pebble conglomerate and sandstone. This coarse fluvial material was deposited at the margin of the Escalante Desert and probably underlies the geothermal area at depth. This unit may have been encountered below a depth of 670 meters (2,200 ft) in the Christiansen (sic) #1 well (CHR-1 on plate 1). It corresponds to the higher density valley-fill material of the gravity model (see later section). Overlying this unit is lower Pleistocene to Pliocene piedmont-slope alluvium (QTpo). This material is poorly to moderately consolidated and consists of boulder, cobble, and pebble conglomerate and sandstone. It contains distinctive, black magnetite clasts derived from the iron deposits of Iron Mountain, located 10 kilometers (6.2 mi) to the east.

Units younger than the semi-consolidated deposits include several types of unconsolidated deposits of Pleistocene age. Stream-terrace alluvium (Qtm) consists of gravel, sand, and silt deposited in stream channels and floodplains at an elevation of approximately 15 to 25 meters (50 to 80 ft) above modern channels. Piedmont-slope alluvium (Qpm) consists of sandy gravel and forms remnants of a dissected surface in older and higher mountain front re-entrants. Alluvial-fan deposits (Qfm) consist of sand and silt that form the dissected remnants of older and higher alluvial-fan deposits in the Escalante Desert. These older fans were largely deposited by an ancestral Pinto Creek.

The youngest unconsolidated deposits consist of sand, silt, gravel, and clay divided on the basis of depositional environment and geomorphic expression. Colluvium and talus (Qct) includes deposits on steep slopes below rock outcrops. Alluvium and colluvium (Qac) includes material deposited in intermittent stream channels and on lower slopes as sheetwash and talus. Distal alluvial-fan deposits (Qpy) in the northwest part of the map consist of silt and clay deposited in the distal parts of the alluvial fans of Pinto Creek and other drainages to the southwest. They are derived principally from sheetwash and stream erosion of the coarser Pleistocene alluvial-fan deposits. Young alluvial-fan deposits (Qfy) are those deposited by Pinto Creek in the Escalante Desert during Holocene and late Pleistocene time. Young stream-terrace alluvial deposits (Qty) occur about 2 to 3 meters (6 to 10 ft) above the modern channel of Pinto Creek and are mostly Holocene in age. Alluvium (Qal) is restricted to modern channels, while artificial fill (Qf) represents the earthen dam of Newcastle Reservoir.

Structure

Structural investigations at Newcastle included mapping of bedrock structures and Quaternary structures, and measurement of slip directions of minor faults from five sites near Newcastle (see next section). The goals of these studies were to document the surface expression of structures that may localize the geothermal resource at Newcastle, to project these structures into the subsurface (plate 1), and to determine the timing and nature of tectonic episodes.

The Antelope Range fault, as defined by Quaternary fault scarps, is a north-northeast-striking normal fault that extends from south of Newcastle to the northern tip of the Antelope Range, a distance of 26 kilometers (16 mi). At Newcastle, the fault separates the Escalante Desert to the northwest from the uplifted bedrock of the Antelope Range to the southeast.

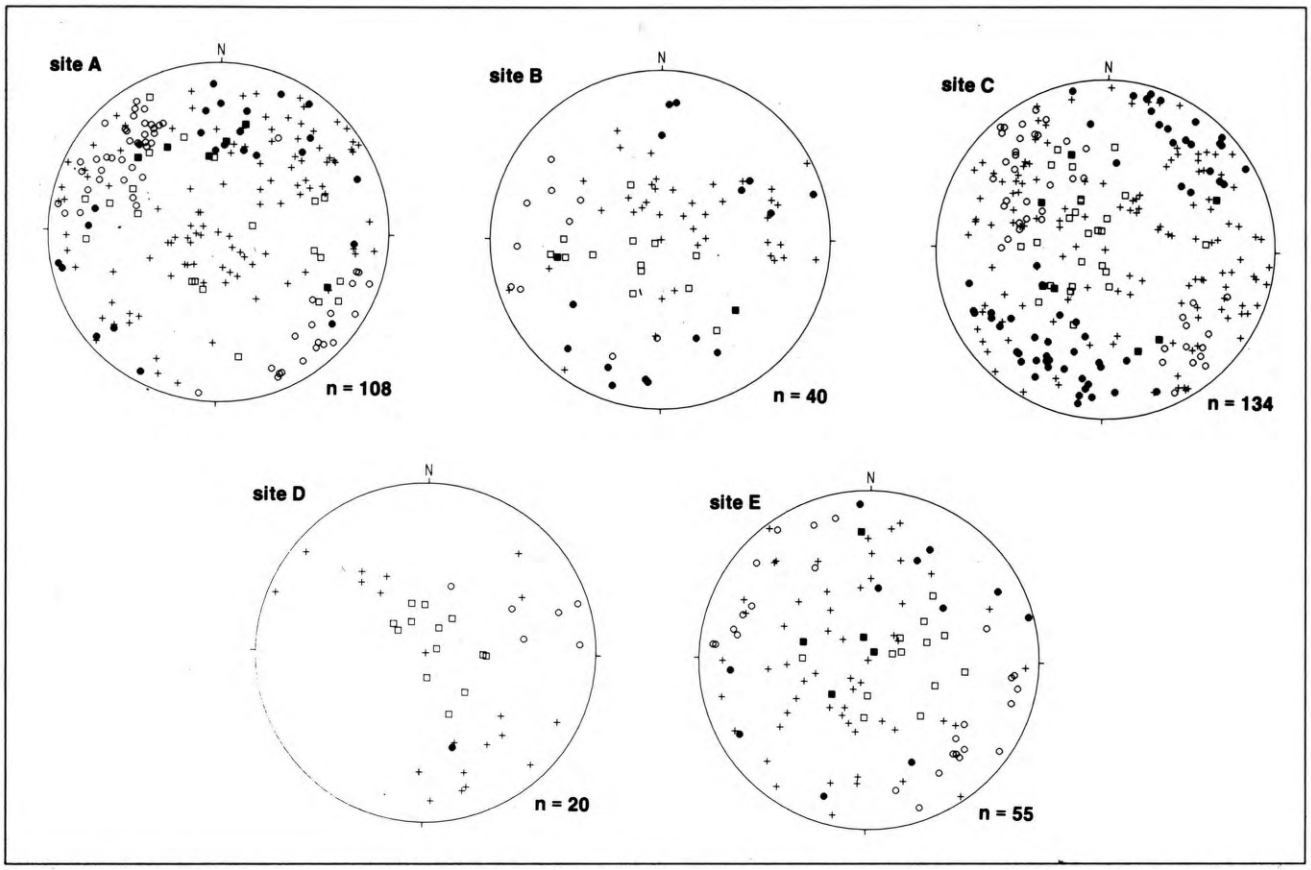

Figure 3. *Summary of fault-slip data from the Newcastle area. Locations of sites shown on plate 1. Symbols corresponding to slip vector orientations are as follows: open circles, dextral faults; filled circles, sinistral faults; open squares, normal faults; filled squares, reverse faults. Plus symbols are poles to fault planes. N is the number of measurements. All nets are lower hemisphere Schmidt projections.*

Although not marked by distinctive Quaternary-age scarps, the fault probably continues an additional 14 kilometers (9 mi) to the southwest, terminating near Mountain Meadow. As mapped by Siders and others (1990), the fault breaks into three right-stepping en echelon strands east of Newcastle (plate 1). Anderson and Christenson (1989) assign a middle to late Pleistocene age for the last surface-rupturing event, based on scarp morphology. Scarps in Pleistocene alluvium northeast of Newcastle, mapped by Grant and Proctor (1988) and Shubat and Siders (1988), are multiple-event scarps. Without additional information, it is not possible to determine if the southwestern limit of Quaternary scarps represents the tip of the most recent surface-rupturing event or if scarps were simply not preserved southwest of Newcastle. Mapping by Siders and others (1990) and Shubat and Siders (1988) shows that the Antelope Range fault cuts 8.5 million year old rhyolite and dacite flows.

Gravity data indicate that the Antelope Range fault marks the southeastern margin of a northeast-oriented, alluvium-filled graben named the Newcastle graben by Pe and Cook (1980). The geothermal system lies along the southeast margin of the Newcastle graben, spatially associated with the Antelope Range fault. This graben, depicted in cross sections B-B' and C-C' (plate 2), is centered approximately 3.7 kilometers (2.3 mi) northwest of Newcastle and contains a thick section of alluvium. Modeling of detailed gravity data (this study) indicates that the dip of the Antelope Range fault is steep (approximately 65 degrees) and that the Newcastle graben contains about 1,600 meters (5,250 ft) of unconsolidated and semi-consolidated material. This corresponds to nearly 1,800 meters (6,000 ft) of dip-slip separation along the fault.

Geologic mapping of the southern extension of the Antelope Range, south and east of Newcastle, revealed a complex pattern of steeply to moderately dipping faults that strike in all directions (plate 1). Geologic cross sections (plate 2) show that these faults probably form an interconnected network of

cross-cutting structures to a depth of several kilometers. Most faults show apparent normal separation, as determined by stratigraphic separation and dips from three-point solutions. However, the dominant displacement on map-scale faults, if similar to minor faults, may be strike-slip, as shown by the dominantly sub-horizontal rakes of minor fault striae at several sites near Newcastle (figure 3). Because of the lack of distinctive, offset features, or geologic lines, we could not determine the net slip for any of the map-scale faults. Stratigraphic separation appears to be the greatest (610 to 910 meters; 2,000 to 3,000 ft) and the most variable along northwest-striking faults and fault zones. One of these faults contains a very coarse breccia body (megabreccia) lying between two fault splays located in the NE ¼ of section 29, T. 36 S., R. 15 W. This is a steep, apparent reverse fault. In the subsurface this brecciated fault zone projects northwesterly toward the center of the thermal anomaly (near holes NC-18 and NC-19, plate 1). Plate 1 shows the map-view projection of this and other faults and contacts onto the footwall of the Antelope Range fault, assuming that the Antelope Range fault dips steeply (65-70 degrees) toward the valley and strikes parallel to its surface trace. This projection shows that the center of the thermal anomaly coincides with an area where two prominent high-angle faults intersect in the plane of the range-front fault.

FAULT-SLIP ANALYSIS

Methods

We conducted a fault-slip study at Newcastle to better characterize the deformational episodes that affected the area and to establish a chronology of these episodes. Fault-slip analysis involves the fitting of a mean stress tensor to a population of fault-slip measurements. Angelier (1979; 1984), Gephart and Forsyth (1984), Angelier and others (1985), and Reches (1987) developed the methods used in this study. To apply this technique, we measured many minor fault orientations from several outcrop-scale areas and for each fault recorded the strike, dip, rake, and sense of slip. These data, converted to a slip-vector format (direction of movement of the hanging-wall with respect to the footwall), are shown in figure 3. Petit (1987) and Angelier and others (1985) document the use of minor structures on fault planes to determine the sense of slip. In this study we found that riedel shears, tension gashes, and corniced margins of void spaces were the most consistent indicators of slip. We found that the Harmony Hills Tuff contained a much higher density of minor fault surfaces than any other unit, probably as a result of favorable physical properties and preservation characteristics. In general, we were able to confidently determine the slip direction for only a fraction (one third) of the minor fault surfaces exposed in the field.

We collected data from five sites, four of which lie within the area of plate 1 (sites A, B, C, and D). Faults at sites A, B, and C cut the 22.5 million year old Harmony Hills Tuff, which yields the maximum age of these faults. Faults at site D cut 8.5 million year old rhyolite and dacite, again yielding the maximum age of this set of faults. The number of faults measured for sites A, B, C, and D are 108, 40, 134, and 20, respectively. A fifth site, site E, located in the $NW\frac{1}{4}NE\frac{1}{4}SW\frac{1}{4}$, section 19, T. 35 S., R. 14 W., yielded 55 measurements. This site lies about 12 kilometers (7.5 mi) northeast of Newcastle in Chloride Canyon and was selected to provide a contrast to the Newcastle sites.

Paleostress tensors for each site (table 1) were determined by a two-stage process consisting of inversion (Reches, 1987) followed by a one-norm measure of misfit minimization scheme (Gephart and Forsyth, 1984) based on the downhill simplex method (Press and others, 1986). Results from inversion were used to seed the downhill simplex minimization. The one-norm minimization approach was adopted because chi-squared tests showed that, for many fault populations, residuals are not normally distributed. Quality of data and the uniqueness of tectonic episodes were assessed by mapping 95 percent and 70 percent confidence limit contours for each stress axis (figure 5), calculated using the one-norm measure of misfit (Gephart and Forsyth, 1984). The confidence limit contour plots may be interpreted as follows: if one were to return to the outcrop where a fault-slip data set was collected and collect a new data set, there would be a 95 percent chance that "best-fit" principal stress axes for the new set would fall within the 95 percent confidence limit contours determined for the old set. A simple graphical method was used to separate heterogeneous fault-slip populations into subsets relating to different tectonic episodes. Modeling of Newcastle field data with synthetic data provided permissive evidence supporting the separation of heterogeneous data.

Table 1. Summary of paleostress tensor determinations for the Newcastle area. The queried tectonic episode (T_3?) reflects uncertainty in the assignment because of the large regions enclosed by confidence limit contours (figure 5c). Site locations (A through E) shown on plate 1. Number in parentheses is the number of faults in population. Axes orientations given in trend and plunge (degrees). Φ, mean slip axis misfit, % data retained, and tectonic episode defined in text. Age of host rock in millions of years.

Fault population	Sub-set	% Data retained	σ_1 Axis (tr/pl)	σ_2 Axis (tr/pl)	σ_3 Axis (tr/pl)	Φ	Mean slip-axis misfit	Age of host rock	Tectonic episode
	A_1(69)		349 16	183 74	80 4	0.39	15.27	22.5	T_1
A(108)		89%							
	A_2(27)		194 61	29 28	295 6	0.93	26.79	22.5	T_3?
B(40)	—	80%	339 22	143 67	247 6	0.77	24.94	22.5	T_1
	C_1(100)		353 5	98 71	262 19	0.40	18.80	22.5	T_1
C(134)		89%							
	C_2(20)		11 75	279 1	189 15	0.26	22.10	22.5	T_2
D(20)	—	100%	31 82	292 1	201 8	0.15	22.34	8.5	T_2
E(55)	—	85%	0 0	268 85	90 5	0.93	32.40	22.5	T_1

A parameter termed the "slip-axis misfit" was used to fit mean paleostress tensors to the fault-slip data collected in the field. The slip-axis misfit is the angle between the observed slip direction and the calculated slip direction for a particular fault and a particular stress model. The mean slip-axis misfit is the average value of the slip-axis misfits for all faults in a population, assuming a particular stress model. The mean slip-axis misfit is the quantity that was minimized in order to find the best-fitting stress model for a fault population. The information required to define a stress model consists of the three directions of the principal stress axes and the ratio of the stress magnitudes (Φ), defined as the quantity $(\sigma_2-\sigma_3)/(\sigma_1-\sigma_3)$.

Results

Table 1 lists the results of the fault-slip analysis. Analysis of data from sites A and C showed that these populations probably consist of a mixture of two populations each, labeled A_1, A_2, C_1, and C_2 in table 1. Fault measurements that had a slip-axis misfit of greater than 90 degrees were deleted from each data set because of the possibility that these data represent faults with misidentified sense of slip. Thus, the percent data retained (table 1) refers to the proportion of measurements in each population with slip-axis misfits less than 90 degrees. Removal of this data did not significantly alter the orientations of the axes of the solution tensors and greatly reduced the mean slip-axis misfits. Many factors probably account for the presence of these high-misfit data, such as slumping of exposures and a failure for some of the faults to meet the assumption of the method. These assumptions are that the deformation occurred under a homogeneous state of stress, that slip along each fault occurred independently, and that slip was in the direction of maximum resolved shear stress.

Figure 4 summarizes the results of paleostress tensor determinations. A preliminary examination of the orientations of least principal stress axes from the seven fault populations (table 1) suggests that they fall into three groups, labeled T_1, T_2, and T_3? in figure

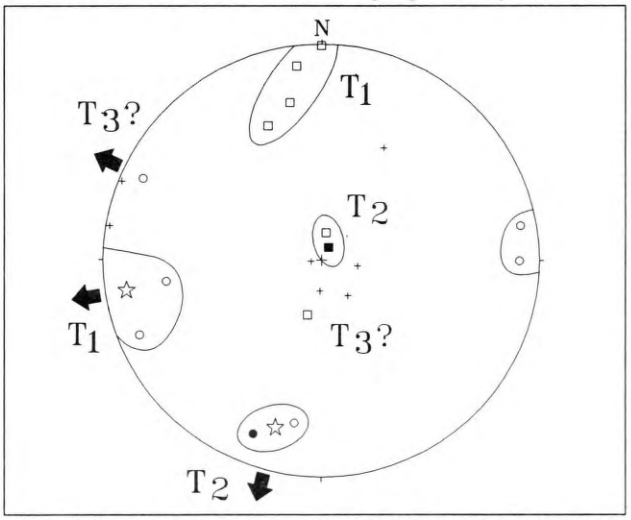

Figure 4. Summary of paleostress axes determinations for the Newcastle area (lower hemisphere Wulff projection). Heavy arrows are the extension directions related to the T_1 and T_2 episodes described in text. Also shown is a possible third episode (T_3?) that was found to be indistinct from the T_1 and T_2 episodes by examination of confidence limit contour plots (figure 5). Open circles, σ_3 axes in 22 million year rocks; solid circle, σ_3 axis in 8.5 million year rocks; open squares, σ_1 axes in 22 million years rocks; solid square, σ_1 axis in 8.5 million year rocks; plus symbol, σ_2 axes; star, "best fit" axes to T_1 and T_2 tectonic episodes (σ_3).

4, which define three apparently distinct tectonic episodes. The T_3? episode, while appearing to have a distinct extension direction compared to the other two episodes was, in fact, found to be so poorly defined as to be indistinct from them (see below). The dominance of extension in the region provides justification for using the least principal stress axes to define tectonic episodes. These episodes are characterized below.

Four of the fault populations, constituting 74 percent of the fault-slip data, are grouped into the T_1 episode. This is clearly the main deformational episode expressed in the minor fault populations. The best-fit least principal stress axis for the T_1 episode has a trend of 261 degrees and a plunge of 6 degrees, which is the eigenvector corresponding to the maximum eigenvalue of the orientation matrix (Mardia, 1972). Maximum principal stress axes for T_1 populations are sub-horizontal, indicating that the T_1 episode consisted of dominantly strike-slip faulting. Confidence limit contours for the T_1 populations are shown in figure 5a. Regions enclosed by the 95 percent confidence limit contours mutually overlap in all cases but one (site B, s_3 axis), providing permissive evidence supporting this grouping of sites into the T_1 episode. The regions enclosed by the 95 percent confidence limit contours for three of the four populations are small relative to other populations (figures 8b and 8c), suggesting that this episode is better defined than the others.

Two fault populations, constituting 11 percent of the fault-slip data, define the T_2 episode. The best-fit least principal stress axis for the T_2 episode has a trend of 205 degrees and a plunge of 19 degrees (eigenvector corresponding to the maximum eigenvalue of the orientation matrix). Maximum principal stress axes for T_2 populations are sub-vertical, indicating dip-slip faulting. Figure 5b shows the confidence limit contours for T_2 populations. The nearly complete overlap of regions enclosed by the confidence limit contours for all three axes supports the grouping of these two populations into the same tectonic episode. The horizontal and overlapping girdle distributions of the regions enclosed by the σ_2 and σ_3 axes' confidence limit contours indicate that these axes can not be clearly distinguished, consistent with the small Φ values obtained for this episode. The non-overlap of confidence limit contours for the respective axes of the T_1 and T_2 populations is strong evidence that these two episodes are distinct and unique.

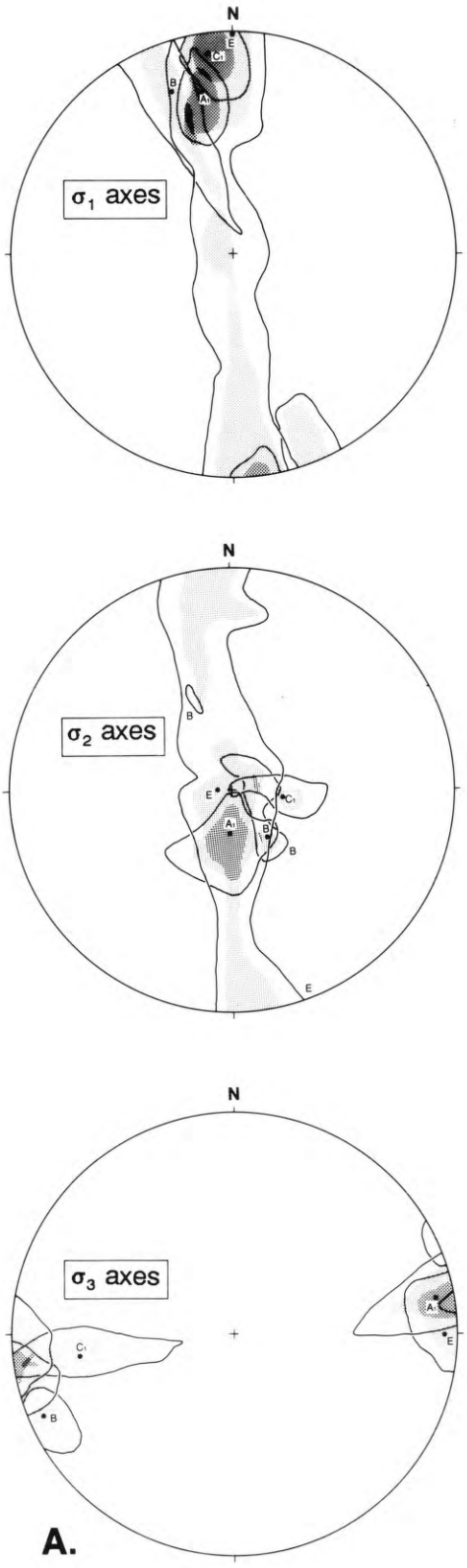

Figure 5. Confidence limit contour plots for Newcastle fault-slip data. Areas enclosed by the 70 percent confidence limit are shaded. Lines are 95 percent

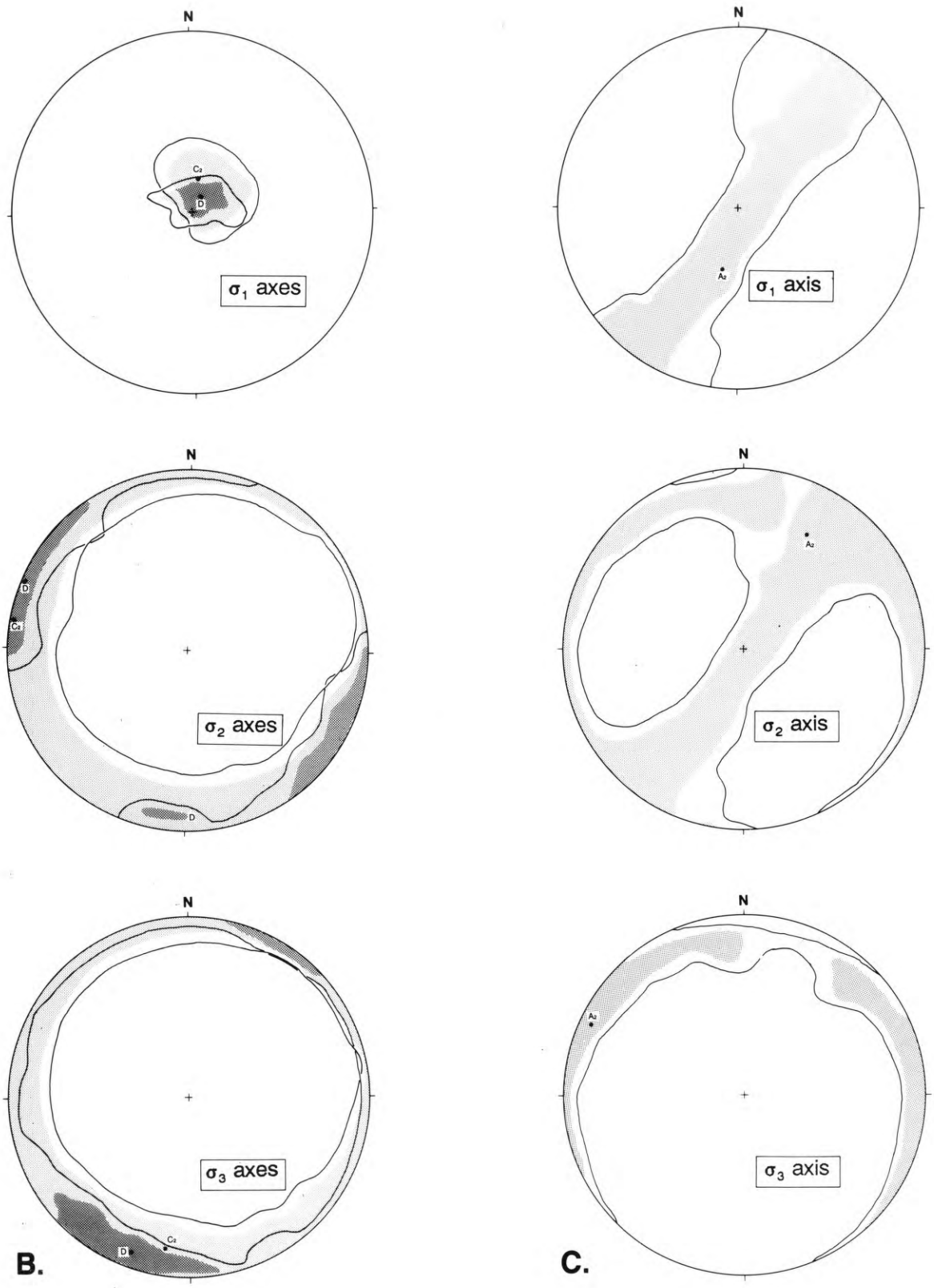

confidence limit contours. Dots are the best-fit principal stress axes from table 1. Letters refer to the fault population designations in table 1. (A) Fault populations assigned to the T_1 episode. (B) Population assigned to the T_2 episode. (C) Population tentatively assigned to the T_3? episode.

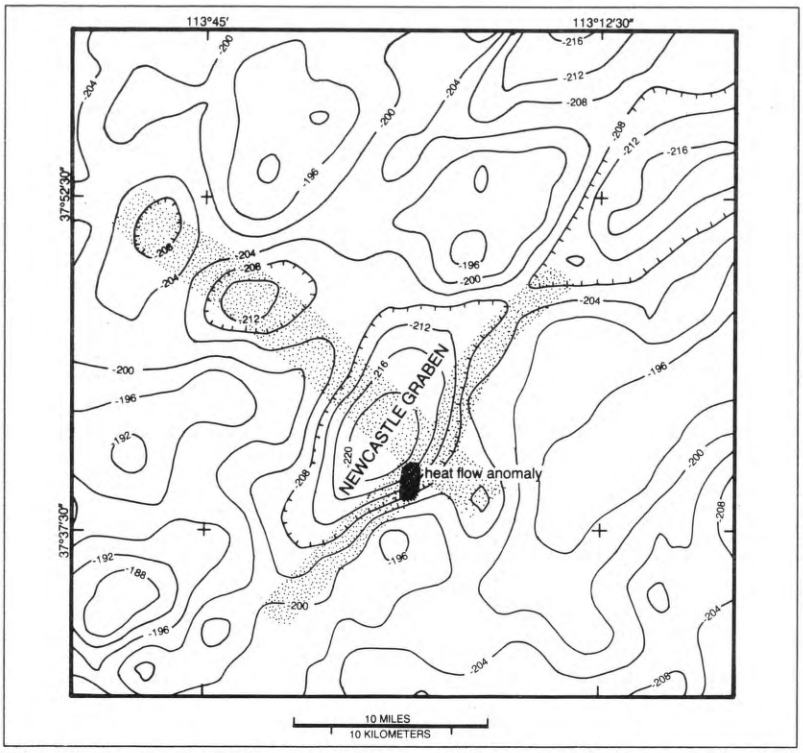

Figure 6. Complete Bouguer gravity anomaly map of the Escalante Valley and vicinity, Utah (contour interval - 4 mgal). Stipple pattern indicates the northwest-southeast alignment of gravity lows and the steep gravity gradient associated with the northeast-southwest-oriented Antelope Range fault. Cross-hatch pattern near the center of the figure shows the general location of the geothermal outflow at Newcastle. Adapted from Pe and Cook (1980).

A single fault population, of 8 percent of the fault-slip data, defines a possible third (T_3?) episode, with a least principal stress axis oriented 299 degrees and plunging 4 degrees. The maximum principal stress axes for the T_3? population is sub-vertical, indicating dip-slip faulting. Girdle distributions of the regions enclosed by confidence limit contours for all axes (figure 5c) indicate that the T_3? episode is not well defined. Confidence limit contours for the axes of the T_3? episode overlap (to a great extent) the respective axes of both the T_1 and T_2 episodes, indicating that the T_3? episode can not be confidently distinguished from the T_1 or T_2 episodes. Thus, scrutiny of figure 5 shows that only two tectonic episodes, the T_1 and the T_2 episodes, can be confidently distinguished using fault-slip data.

Timing of Tectonic Episodes

Definition of the T_1 episode using data collected from the 22.5 million year Harmony Hills Tuff (sites A_1, B, C_1, and E, table 1) and the absence of this mode of faulting from data collected from the 8.5 million year old rhyolite of Silver Peak (site D) suggest that most of the deformation associated with the T_1 episode occurred between 22.5 and 8.5 million years. Three arguments suggest that most of the map-scale faults cutting bedrock units (plate 1) in the Newcastle geothermal area formed during the T_1 episode. First, reconnaissance fault-slip data from the area were collected from exposures of map-scale faults and yield paleostress tensor results consistent with the T_1 episode. Second, two of the detailed sampling sites (sites A_1 and C_1) used to define the T_1 episode lie in the hanging walls of mapped faults in close proximity to the fault traces. Mapping in these areas showed that the density of minor faults at both sites decreases markedly with increasing distance from fault traces. Thus the minor faults at these sites are probably genetically related to the map-scale faults. Third, two piercing-point reconstructions in the northeast corner of the Silver Peak 7½' quadrangle (Shubat and Siders, 1988) yielded results compatible with calculated slip directions using the stress tensor of the T_1 episode.

The age of the T_2 episode is not as well defined as the T_1 episode. One of the fault populations used to define the T_2 episode occurs in 8.5 million year old rhyolite, indicating that the T_2 episode is at least in part post-8.5 million years in age. No mapped structures can be uniquely associated with the T_2 episode and the relationship between this episode and mapped structures remains unresolved.

Summary of Fault-Slip Analysis

Fault-slip data indicate that the oldest episode (T_1) at Newcastle consisted of dominantly strike-slip extensional faulting with the axis of least principal stress oriented WSW. Field relations indicate that this episode produced most of the map-scale faults cutting bedrock at Newcastle and the age of the episode is middle to late Miocene. The T_1 episode at Newcastle is similar in timing and extension direction, and thus probably correlative with, a widely recognized middle Miocene episode of regional extent in southeastern Nevada and adjacent parts of Utah (Zoback and others, 1981; Anderson, 1989; Angelier, 1989). The T_2 episode is well defined by fault-slip data but is not expressed as a unique struc-

tural style and its regional significance is unknown. The origin of the Antelope Range fault remains ambiguous. Normal slip on the fault is incompatible with the paleostress tensors determined in this study (the T_1 and T_2 episodes), leading to two possible interpretations. First, if the Antelope Range fault has had a history of dominantly normal slip, it is possible that this episode did not produce a significant number of minor faults and that the episode was not detected by the fault-slip study. Second, it is possible that net slip on the Antelope Range fault is left-oblique, forming (in part at least) in response to the T_1 episode, and that net slip on the fault is several times the vertical component of separation (greater than 1.6 km). Mapping of Quaternary units in the Newcastle area (Siders and others, 1990) and a Quaternary fault study (Anderson and Christenson, 1989), however, provide no evidence supporting left-oblique slip since Pleistocene. We conclude that formation of the Antelope Range fault postdates formation of the mapped faults cutting bedrock and that there has been little reactivation of faults, map-scale or minor faults, during uplift of the range (late Miocene or Pliocene to present).

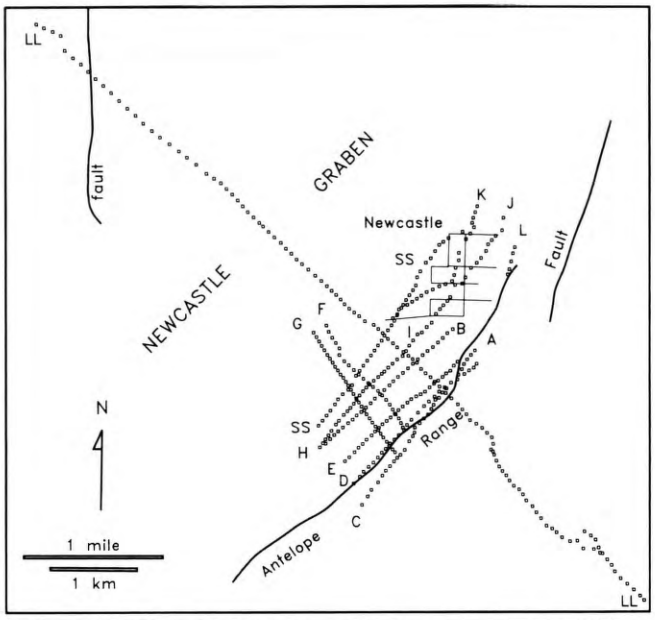

Figure 7. Detailed gravity survey station locations, lines SS, LL, and A through K.

GRAVITY STUDIES

Detailed Surveys

Previous gravity investigations of the Escalante Desert and vicinity (figure 6) focused on regional gravity and tectonic patterns in the Great Basin (Eaton and others, 1978; Pe, 1980; and Pe and Cook, 1980). C.M. Schlinger and students of the University of Utah Department of Geology and Geophysics completed detailed gravity surveys at Newcastle as part of this study (Blackett and others, 1990). Because the control of fluid movement in geothermal systems is often directly related to fracture permeability, Schlinger designed the detailed surveys to determine the geologic structure beneath the alluvial fill of the Escalante Desert. Goals of the gravity studies were to (1) estimate the dip of the Antelope Range fault, (2) detect the presence of any hanging-wall structures, and (3) to estimate the depth to bedrock beneath the Escalante Desert. The surveys, performed during

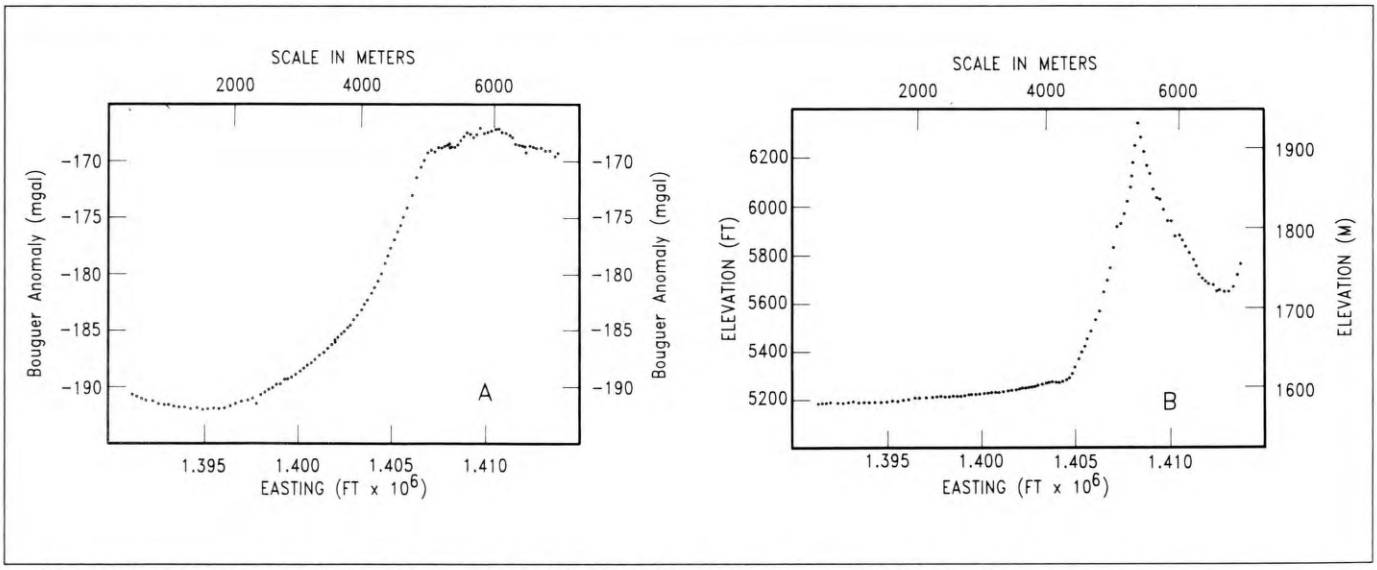

Figure 8. Bouguer gravity anomaly (A) and station elevations (B) along line LL. Easting values are state plane coordinates.

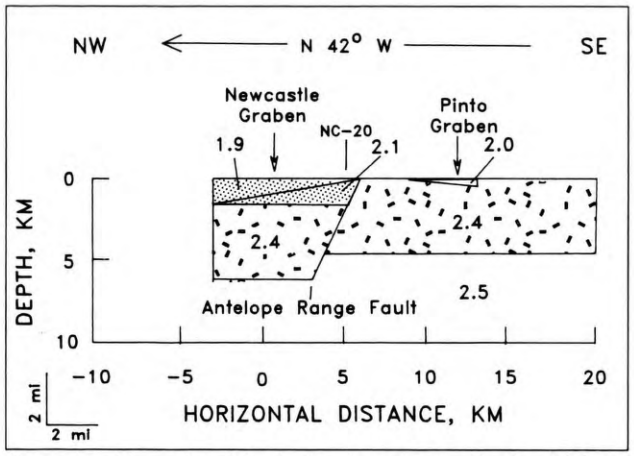

Figure 9. Forward model of subsurface structure in the vicinity of Newcastle. Densities are in g/cm³. Polygonal cross-section structures have strike lengths of 20 kilometers (12.5 mi), except for the Pinto graben which has a strike length of 4 kilometer (2.5 mi). Zero km mark corresponds to the northwest end of line LL.

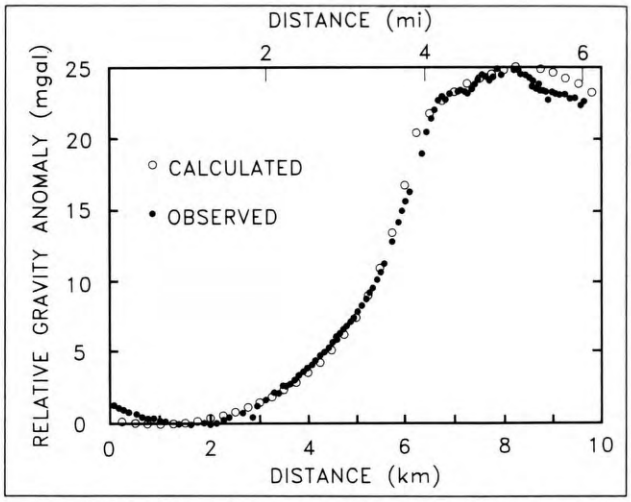

Figure 10. Comparison between observed and calculated gravity anomaly of figure 9.

November of 1987 and September of 1988, consisted of close-spaced (8 m) gravity measurements along traverses oriented both parallel and normal to the Antelope Range fault (figure 7).

A local gravity base station (GBS) was established approximately 15 meters (50 ft) south of the Newcastle cemetery, about 1.6 kilometers (1 mi) west of the town center. The survey teams determined absolute gravity at GBS and at all gravity survey points by tying to the regional gravity base station located in Enterprise. Cook and others (1971) established this gravity base station as a regional reference point. Schlinger and students used two portable La Coste and Romberg gravity meters for the survey. Diurnal variation of the earth's gravity field along with instrument drift over time were determined by repeating readings every three to five hours at GBS with each gravimeter. Survey crews took gravity measurements at 393 stations during two surveying periods. Station locations and elevations were determined using a combination theodolite and electronic distance meter. Surveyed points were tied to established USGS bench marks and section corners (Blackett and others, 1990, p. 23).

Reduction of Gravity Data

Using observed gravity measured at each station, the field teams determined the complete Bouguer anomaly by standard methods described in Telford and others (1976) and Dobrin and Savit (1988). Figure 8 shows station locations, station elevations, and the Bouguer anomaly for gravity survey line LL (figure 7), a long profile normal to the Antelope Range fault. The Bouguer anomaly and station elevations are plotted as a function of the easting (Utah state plane) coordinates. The principal variations in Bouguer gravity relate to the offset of bedrock units by the Antelope Range fault (figure 8a). Low values on the left hand side of the diagram reflect low-density materials filling the Newcastle graben. High values on the right hand side of the diagram reflect the presence of high-density volcanic and sedimentary rock units present in the adjacent range.

In order to estimate dip and total offset along the Antelope Range fault, Schlinger modified a 2.5 dimensional forward-modelling routine written by J.H. Luetgert of the USGS, based on the algorithm of Cady (1980). Schlinger's modifications allow the routine to operate on UNIX-based and PC-type computers. The 2.5 dimensional algorithm uses constant-density horizontal prisms that are polygonal in cross section. The cross-section shapes and densities do not vary along the strike lengths of the prisms. The strike lengths of the prisms are finite.

Interpretation of Gravity Studies

Figure 9 illustrates the results of forward modeling. The model approximates the gravity profile along line LL. Rocks forming the lower layer of the model, assumed to be Mesozoic sedimentary rocks, are represented with a density of 2.5 g/cm³ (156 lbs/ft³). Overlying sedimentary rocks of the Iron Springs and Claron Formations, and volcanic rocks of the Isom Formation and Quichapa Group and unnamed

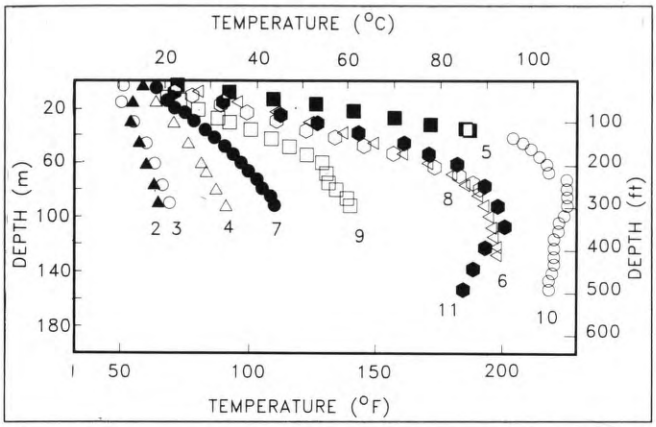

Figure 11. *Temperature-depth plots for wells NC-2 through NC-11. From Clement (1981) and Chapman and others (1981).*

volcanic units, are represented by offset prisms, each with a density of 2.4 g/cm³ (150 lbs/ft³). A diagonal line with a dip of 65 degrees to the northwest represents the Antelope Range fault. Two low-density wedges left of the fault, depicting valley-fill material, represent the Newcastle graben. The lower wedge of alluvium, with a density of 2.1 g/cm³ (131 lbs/ft³), thins basinward, and the upper wedge, with a density of 1.9 g/cm³ (119 lbs/ft³), thickens basinward. A thin wedge of alluvial-fan material with an average density of 2.0 g/cm³ (125 lbs/ft³) represents the small "Pinto graben" (Pe, 1980). The strike length of all prisms, except for the Pinto graben, is 20 kilometers (12.4 mi). The prism which represents the Pinto graben has a strike length of 4 kilometers (2.5 mi).

Figure 10 compares the observed data and the calculated gravity anomaly. Varying the fault dip during iterative modeling showed moderate effects to the model. Fault dips ranging from 60 to 70 degrees yield model results that adequately fit the observed data. The model adopted, shown in figure 9, uses a dip of 65 degrees along the Antelope Range fault with total offset of about 1.6 kilometers (1 mi). The model also indicates that the fault may persist to at least 5 kilometers (3 mi) depth.

HEAT FLOW

Working Model

The working model of the Newcastle system in Blackett and others (1990) presumed that meteoric water from recharge areas becomes heated during deep circulation in a region of elevated heat flow (about 90 mW/m²). This model includes a zone of high permeability, located at the contact between valley fill and bedrock, that provides a preferred pathway for upflow and localized discharge of heated ground water to the valley-fill deposits. The model also suggests that minerals, precipitating from geothermal fluid within alluvium in the deep parts of the Newcastle system, may form a low-permeability barrier (or seal) that prevents thermal fluid from moving basinward. Such a barrier would enhance the upward flow of thermal fluid near the bedrock-alluvium contact. Fine-grained (clay-rich) materials that fill void spaces within coarse-grained alluvium adjacent to the Antelope Range fault might also create a low-permeability barrier. Thermal water from this up-flow zone, which discharges into a shallow aquifer, probably mixes with cool ground water in alluvial-fan deposits along the southeast margin of the Escalante Desert.

Thermal Studies

Figure 11 illustrates plots of temperature-depth profiles from shallow wells drilled prior to our study (labelled NC-2 through NC-11 in figure 12). The profiles exhibit many features such as subnormal gradients, concave downward curvature, isothermal sections, and temperature reversals that are characteristic of many geothermal systems (Bodvarsson, 1973; Lachenbruch and others, 1976; Sass and Sammel, 1976; Lachenbruch and Sass, 1978; Mase and others, 1978; Sorey and others, 1978). These types of features are caused by fluid movement in zones of recharge (downward flow), discharge (upward flow), and lateral flow where heat is transferred by moving ground water. Drill hole NC-12, located about 3 kilometers (1.8 mi) northeast of Newcastle (not shown in figures 11 and 12), exhibits a subnormal gradient (21°C/km; 1.1°F/100 ft) indicative of a hydrologic recharge zone. The remaining drill holes exhibit high near-surface gradients ranging from 89°C/km (4.8°F/100 ft) to 1,870°C/km (101.1°F/100 ft). Drill holes NC-2, 3, and 4 exhibit constant temperature gradients. The temperature profiles for drill holes NC-6, 10, and 11 become isothermal, or show a temperature gradient reversal, between 75 and 100 meters (246 and 328 ft). These patterns led Chapman and others (1981) to conclude that heated ground water flows laterally at shallow depths generally between 75 and 100 meters (246 to 312 ft) in a more permeable zone, denoted here as an "out-flow plume." Heat is released from this region of elevated temperature mainly by

conduction into the surrounding lower temperature material and by mixing with cooler ground water.

Union Geothermal Division (UNOCAL Corporation) contributed unpublished results of thermal, geophysical, and lithology logging for a deep exploration well (Christiansen #1, designated here as CHR-1, figures 12 and 13). Temperatures in CHR-1 exceeded 120°C (248°F) between depths of 79 meters and 183 meters (259 ft and 600 ft), and the maximum temperature was 130°C (266°F) at a depth of 105 meters (346 ft). Near-isothermal conditions with temperatures between 114°C to 119°C (237°F to 246°F) were measured between 183 meters and 912 meters (600 ft and 2,992 ft). Because the temperature log displays a temperature reversal at shallow depth (106 m; 348 ft), it was assumed that CHR-1 penetrated a tongue of heated ground water rather than the main upflow zone. If this assumption is correct, then temperatures greater than those observed in CHR-1 could exist at shallow depth in the center of the upflow zone.

Chapman and others (1981) constructed a heat-flow map using the temperature-gradient data for drill holes NC-2 through NC-12 and from three irrigation wells. Heat-flow maxima exceeded 3,000 mW/m² at NC-5 and NC-10. Assuming a background flux of 100 mW/m², they computed a minimum anomalous heat loss of 12.8 MW within an area of 9.4 square kilometers (3.7 mi²) bounded by the 500 mW/m² contour. They also determined that the minimum volume discharge required to create the estimated heat loss was 0.032 m³/s (507 gal/min). Rush (1983) independently estimated a similar but lower volume discharge of 0.013 m³/s (206 gal/min) and proposed a reservoir temperature between 140°C to 170°C (284°F to 338°F) based on the results of chemical analyses of ground water samples.

Although the heat-flow map was poorly constrained in some respects, it suggested the presence of a thermal plume of heated ground water moving to the

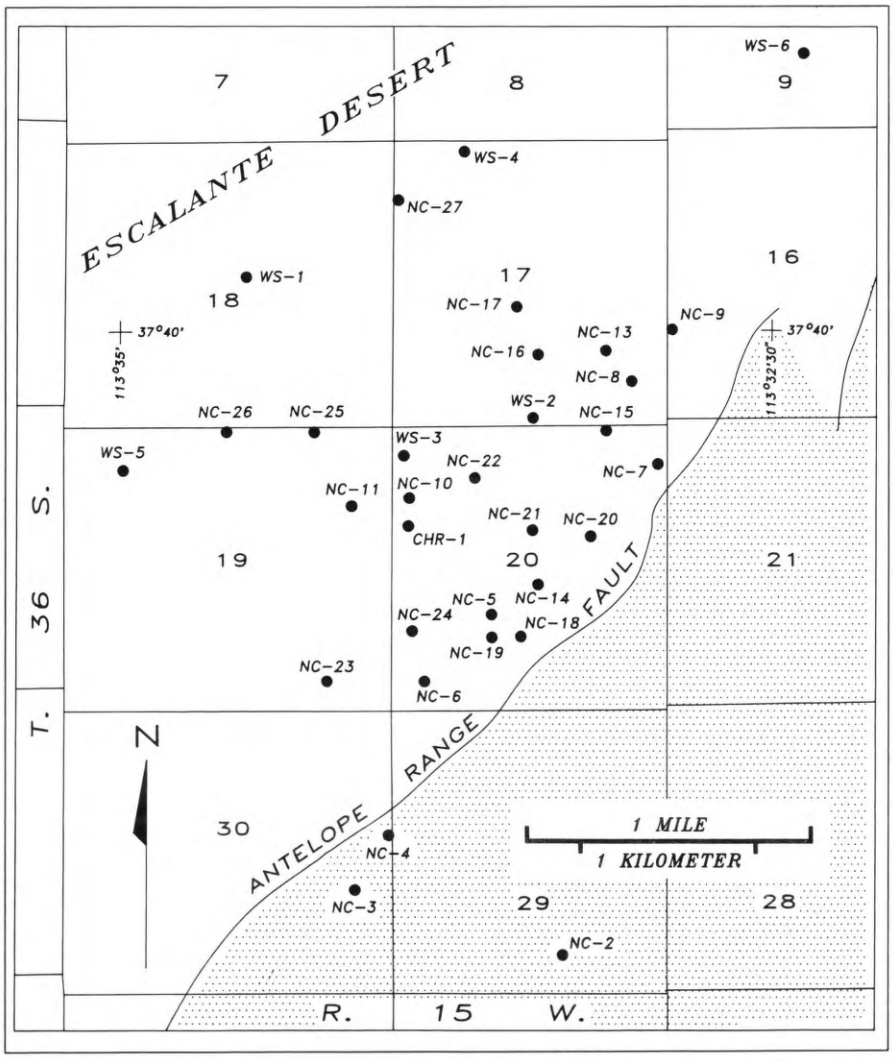

Figure 12. Locations of geothermal wells and temperature-gradient drill holes in the Newcastle study area. Holes drilled prior to this study are designated NC-2 through NC-12. Deep geothermal test drilled by Unocal Geothermal Division is designated CHR-1. Thermal-gradient drill holes monitored for this study are designated NC-13 through NC-27. Wells sampled for water analyses are designated by a "WS" prefix.

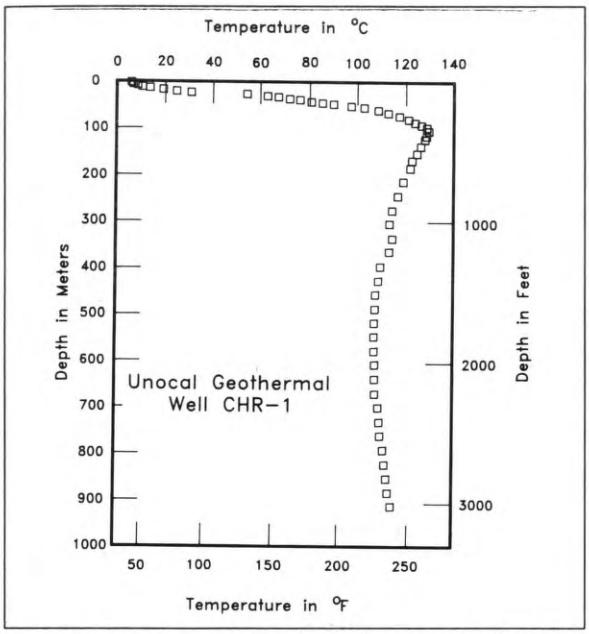

Figure 13. *Temperature-depth plot for Unocal geothermal well CHR-1.*

Table 3. *Heat loss for the Newcastle geothermal system.*

Heat flow contour interval (W/m^2)	Area ($10^8 m^2$)	Average heat flow (W/m^2)	Heat loss (MW)
0.5 to 1.0	3.1	0.75	2.3
1.0 to 1.5	1.8	1.25	2.2
1.5 to 2.0	1.5	1.75	2.6
2.0 to 3.0	0.83	2.50	2.1
3.0 to 6.0	0.64	4.50	2.9
6.0 to 9.0	0.10	7.50	0.8
> 9.0	0.033	9.00	0.3
Total	8.0		13.2
Background Heat loss	8.0	0.10	0.8
Heat loss above background			12.4

[1 watt (W) = 1,000 milliwatts (mW)]
[$10^8 m^2$ = 10.76 x $10^8 ft^2$]
[1 megawatt (MW) = 1,000,000 watts (w)]

Table 2. *Temperature-gradient, thermal-conductivity, and heat-flow data for thermal monitoring wells NC-2 through NC-27. Data for NC-2 through NC-12 are from Chapman and others (1981). Data for NC-13 through NC-27 are from Blackett and others (1990).*

[1 watt (W) = 0.2389 calorie/second] [1°C/km = 0.0541°F/100 ft] [1 watt (W) = 1,000 milliwatts (mW)] [1 HFU (heat flow unit) = 41.8 mW/m²] [1 m = 3.281 ft]

Drill Hole or Well	Depth Interval (meters)	Thermal Gradient (°C/km)	Thermal Conductivity (W/m°C)	Heat Flow (mW/m^2)
NC-2	46 to 89	89	2.27	200
NC-3	46 to 89	116	1.70	200
NC-4	8 to 40	220	1.70	370
NC-5	8 to 20	1998	1.70	3400
NC-6	5 to 38	1065	1.73	1840
NC-7	8 to 47	370	1.70	630
NC-8	17 to 41	1028	1.70	1750
NC-9	8 to 56	710	1.70	1210
NC-10	0 to 40	1833	1.76	3230
NC-11	15 to 46	1292	1.74	2250
NC-12	49 to 118	21	1.70	40
NC-13	5 to 20	729	1.70	1240
NC-14	0 to 14	>5000	1.72	>8600
NC-15	5 to 40	1010	1.68	1700
NC-16	5 to 18	931	1.80	1680
NC-17	5 to 18	847	1.67	1410
NC-18	0 to 13	5737	1.83	10500
NC-19	0 to 14	4615	1.83	8450
NC-20	5 to 20	1409	1.70	2400
NC-21	5 to 18	1943	1.64	3190
NC-22	5 to 18	1267	1.57	1990
NC-23	5 to 18	582	1.80	1050
NC-24	5 to 17	1914	1.55	2970
NC-25	5 to 18	982	1.72	1690
NC-26	7 to 18	521	1.54	800
NC-27	5 to 18	412	1.60	660

north from a source located near the mountain front (Chapman and others, 1981; Rush, 1983). To refine the working model for the system, an evaluation program consisting of shallow temperature gradient drilling and chemical analyses of fluid samples was undertaken (Blackett and others, 1990).

Additional temperature-gradient drilling could locate the center of the upflow zone, delineate its extent, and determine the geometry of the outflow plume. On the basis of the previous temperature-depth data, it was argued that only holes drilled to a depth of 120 to 150 meters (395 to 490 ft) could detect a temperature overturn. It was also noted, however, that shallower holes generally express linear temperature gradients that characterize the conductive, near-surface heat flow. Boreholes drilled to a depth of 18 meters (60 ft) were selected as being sufficiently deep to avoid the "noise" of annual surface temperature variations, but yet an adequate depth to map the conductive heat loss over the top of the geothermal system. Choosing this shallow drill depth would also allow the drilling of a greater number of boreholes while keeping the drilling costs to a minimum.

Twelve shallow (18 meter; 60 ft) thermal-gradient holes were completed at strategic locations. Figures 12 and 14 show the

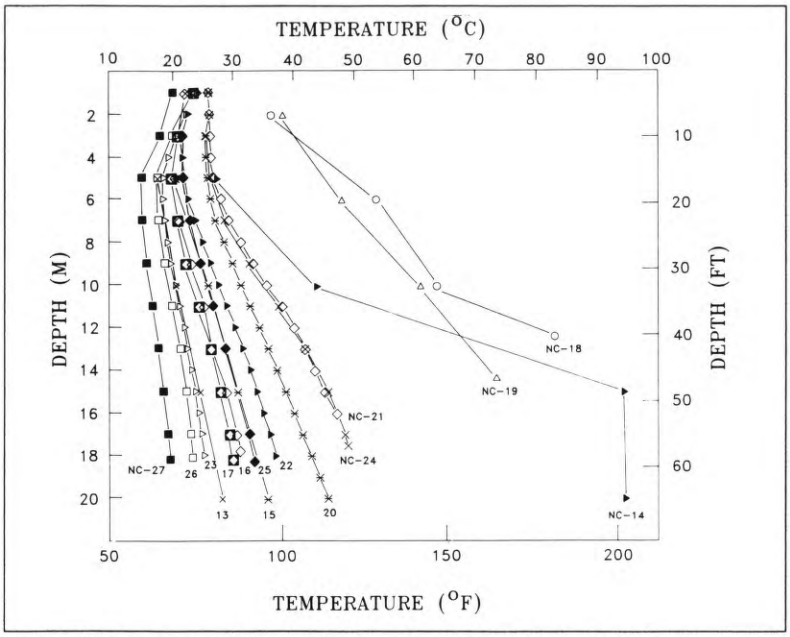

Figure 14. Temperature-depth plots for thermal-gradient drill holes NC-13 through NC-27.

locations of these drill holes and their temperature profiles, designated NC-16 through NC-27. The 12 new holes, drilled with rotary equipment, range in depth from 18 to 21 meters (60 - 70 ft). A bottom-capped, 3.18-centimeter (1.25-inch) ID schedule 40 PVC pipe was inserted in each borehole to total depth, the annulus of the drill hole was filled with drill cuttings, and the PVC pipe was filled with water. Temperature profiles were recorded for the new drill holes and for three existing water wells drilled by other parties, designated NC-13, NC-14, and NC-15 (figures 12 and 14).

Temperatures were measured in each drill hole at depth intervals ranging between 1 and 5 meters (3.3 and 16.4 ft) three times over a period of nine months. The temperature probe consisted of a thermistor connected by four-wire cable to a digital ohmmeter. The thermistor was a Fenwal K212E with a nominal 10,000 ohm resistance at 20°C (68°F), a power dissipation of 50 milliwatts/°C in still water, and a response time of 7seconds. The therrmistor was calibrated against a Hewlett Packard digital quartz thermometer. Precision of the probe was 0.004°C. Accuracy of the temperature measurements considering calibration errors, field conditions, and ohmmeter resolution is 0.01°C.

Due to very slow equilibration time in air, an effort was made to log water-filled drill holes wherever possible. Measurements made in air, above the water table in unsealed holes, require several tens of minutes or longer to approach thermal equilibrium. In these instances, a temperature-time series was obtained at each depth by measuring temperature every 20 seconds for a 5-minute period. Equilibrium temperatures were then determined for those depths using the extrapolation method of Parasnis (1971).

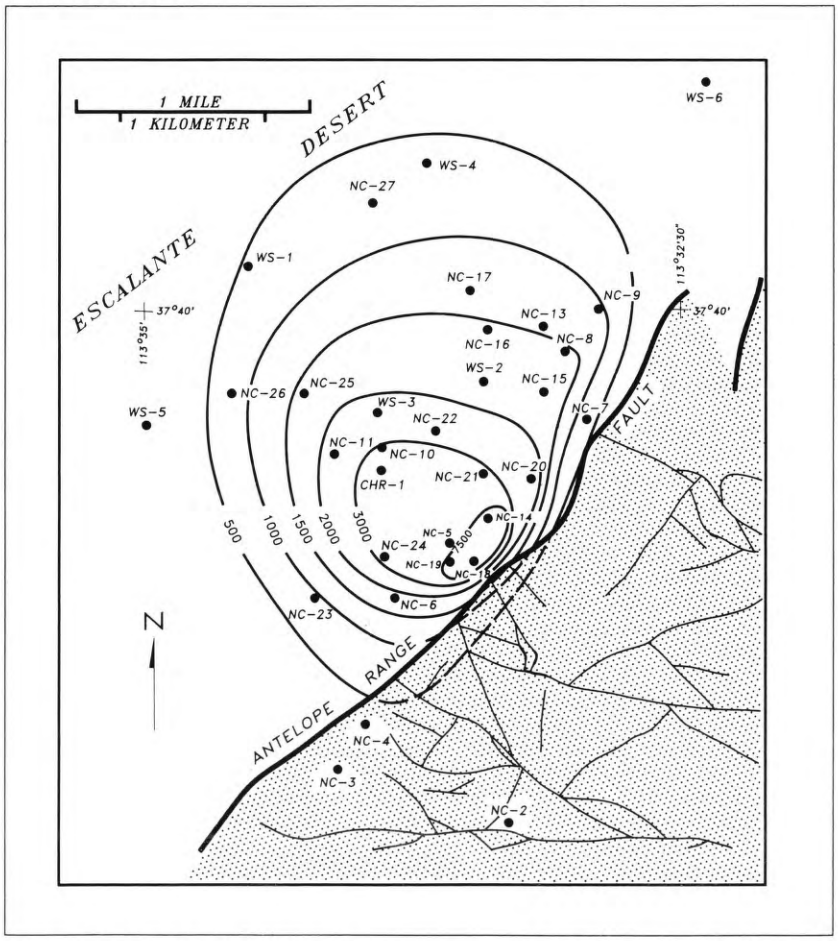

Figure 15. Heat-flow map for the Newcastle geothermal system showing thermal-gradient boreholes and the approximate surface trace of the Antelope Range fault. Heat-flow contours are expressed in milliwatts per square meter (mW/M^2) and heat flow values are presented in table 2. The locations of mapped bedrock faults are indicated by heavy lines in the southeast quadrant of the map. The stipple pattern indicates the general area of exposed bedrock units. Detailed geology is shown on plate 1.

Figure 14 shows temperature-depth profiles for the 15 new holes, designated NC-13 through NC-27. The main feature observed from the new drill holes is the very high, near-surface geothermal gradient seen in boreholes drilled on an alluvial fan southeast of well NC-10 (figure 12, plate 1). Gradients in three drill holes (NC-14, NC-18, and NC-19) over the upper 15 meters (49 ft) are about 5,000°C/km (270°F/100 ft). Although holes NC-18 and NC-19 were drilled to a depth of 18 meters (60 ft), the holes could only be logged to about 12 meters (40 ft), presumably because the PVC casing lost strength and collapsed at temperatures above 70°C (158°F). NC-14, completed with 2.5-centimeter (1-inch) ID black iron pipe, exhibits a high near-surface gradient, achieves a temperature maximum of 94°C (201°F) at a depth of 15 meters (49 ft), and becomes isothermal to total depth at 66 meters (215 ft). Because none of these three holes intersected the water table, with the possible exception of NC-14, this observed temperature field is puzzling. We considered the possibility that the deeper, open-hole portion of NC-14 could be acting as a "chimney," providing for efficient vapor (steam) transport to the near-surface (< 14 meters; 46 ft) environment, or that boiling water convecting lower down in the pipe could produce the isothermal condition. The extremely high thermal gradients observed in NC-18 and NC-19 (shallow air-filled holes completed with plastic pipe) suggest that the thermal field seen in NC-14 is not simply a well-bore effect. Rather, it is a property of this part of the geothermal system. It is speculated that the isothermal temperature field at 94°C (201°F) may result from vapor circulating within the alluvial fan at or near the boiling point of water at this elevation (about 1,646 meters; 5,400 ft), with the upper 15 meters (49 ft) being a conductive boundary on the vapor system.

The curved temperature profiles in the uppermost 6 meters (20 ft) of the temperature-gradient boreholes shown on figure 14 are transient effects of the annual temperature variation at the ground surface and are not important in understanding the geothermal system. Between depths of 6 and 20 meters (20 and 66 ft), however, most of the profiles are linear, indicating that heat transfer through this region is dominantly by conduction. The variability seen in these shallow temperature gradients is directly related to heat loss from the geothermal system.

Heat-flow values were determined by combining thermal-gradient data with thermal conductivity, either measured from drill cuttings or interpolated from nearby wells (Blackett and others, 1990, p. 53). A porosity of 30 percent was assumed in order to compute the bulk conductivity of the alluvial-fan material. Table 2 lists the thermal gradient, thermal conductivity, and computed heat flow. The revised heat-flow map for the Newcastle geothermal system is shown in figure 15.

Drill holes NC-26 and NC-27 exhibited the lowest heat flow values, indicating a northwest limit to the geothermal system (figure 15 and table 2). Similarly, drill holes NC-20 and NC-23 provided control for mapping the northeast and southwest portions of the geothermal system, respectively. Drill holes NC-13, NC-15, NC-16, and NC-17, all situated near the western edge of the town of Newcastle, show that the town itself is situated over a distal part of the outflow plume. Temperature gradients in drill holes NC-14, NC-18, and NC-19 indicate that the hottest, central part of the geothermal system is situated about 1.2 kilometers (0.75 mi) southeast of the discovery well (NC-10), near the trace of the Antelope Range fault. This spatial association provides strong evidence that the range-bounding fault controls the movement of geothermal water.

The heat loss (table 3) for the Newcastle geothermal system was calculated by integrating the anomalous flux over the heat-flow map shown in figure 15. The anomalous heat loss above the background heat flow of 100 mW/m^2, contained within the 500 mW/m^2 contour, was 12.4 MW. This value was slightly less than the previously computed value by Chapman and others (1981) of 12.8 MW because of better control from the additional drilling. A fluid discharge rate of 0.031 m^3/s (490 gal/min) was calculated based on the new estimates of heat loss and by using the previous parameters of Chapman and others (1981).

FLUID CHEMISTRY

Hydrochemistry

Table 4 lists chemical analyses of six groundwater samples collected from local wells (shown in figure 12). Samples WS-2 and WS-3 are from two of the wells that produce hot water for use in commercial greenhouses, the Hildebrand well and the Troy Hygro well, respectively. We obtained samples WS-1, WS-

Table 4. Chemical analyses of ground-water samples from the Newcastle area. ND – not detected; I = inductively coupled plasma spectrometer; T = titration; S = specific ion electrode; B = turbidimetric; G = gravimetric; H = method of Hem (1970); M = pH meter.

Species	Method	Concentration (ppm) WS-1	WS-2	WS-3	WS-4	WS-5	WS-6
Na^+	I	24.58	273.28	290.24	249.61	63.98	104.80
K^+	I	2.76	15.24	16.97	11.74	2.64	5.05
Ca^{2+}	I	54.05	64.57	78.68	64.36	63.82	62.34
Mg^{2+}	I	25.57	0.75	0.69	5.51	25.59	13.32
Fe^{2+}	I	ND	ND	ND	ND	ND	ND
Al^{3+}	I	ND	ND	ND	ND	ND	ND
SiO_2	I	42.12	79.19	69.37	63.24	31.89	46.80
B	I	ND	0.34	ND	0.62	0.15	0.19
Li^+	I	0.50	0.52	0.60	0.33	ND	0.09
Sr^{2+}	I	ND	1.30	1.56	0.36	0.55	0.35
HCO_3^-	T	181.00	58.00	44.00	104.00	182.00	228.00
CO_3^{2-}	T	ND	ND	ND	ND	ND	ND
Cl^-	T	48.00	69.00	104.00	76.00	44.00	82.00
F^-	S	0.30	7.30	6.30	4.70	0.48	1.03
SO_4^{2-}	B	82.00	569.00	637.00	478.00	208.00	115.00
		Total Dissolved Solids (ppm)					
measured (m)	G	364	1154	1236	1016	530	545
calculated (c)	H	369	1109	1227	1005	530	543
100*(m/c)		99	104	101	101	100	100
pH	M	7.74	8.03	7.98	7.89	7.48	7.60
Balance (meq/l)		-0.092	0.538	-0.085	0.831	-0.427	0.417
Temperature (°C)		cold	77	63	32	cold	cold

5, and WS-6 from cold-water irrigation wells and sample WS-4 from a warm-water well. Samples 1, 4, 5, and 6 were taken from actively flowing irrigation wells and are fairly representative of water within the aquifer.

Sample number WS-2 was taken from one of two geothermal wells supplying the Hildebrand greenhouses. Although the pumping system was active, the well was not flowing prior to sampling. The fluid sample was collected after opening a valve near the wellhead and allowing fluid to flow for a few minutes. The sample temperature was 77°C (171°F).

Sample number WS-3 was taken from the supply well for the Troy Hygro System's greenhouses. The well had been shut off probably for several hours until just prior to sampling. The sample collection point was located roughly 100 meters (328 ft) south of the well at the discharge point where the spent fluid discharges into the settling pond. The Troy Hygro manager turned on the well pump, and the well flowed for several minutes until mechanical problems developed. Because the pump needed to be shut off, the manager notified us and the fluid sample was taken just prior to the shut off.

All samples were filtered using a peristaltic pump and 0.45 micron filters. Each sample was collected in two polyethylene bottles. One 500 milliliter (17 fl oz) bottle contained raw filtered sample. The other 32 milliliter (1 fl oz) bottle contained filtered and acidified, one percent HNO_3 sample. Geochemists at the Earth Science Laboratory, University of Utah Research Institute, analyzed the samples using the methods indicated on table 4.

Water analyses plotted on a trilinear diagram (figure 16) indicate that samples WS-2, WS-3, and WS-4 have similar chemistry, and consist of SO_4-Cl-HCO_3 (sulfate-chloride-bicarbonate) type water. Sample WS-1, however, exhibits a much lower value for total dissolved solids (TDS) and is a HCO_3-SO_4-Cl (bicarbonate-sulfate-chloride) type water. This difference in water chemistry suggests that samples WS-2, 3, and 4 contain a component from the geothermal system while sample WS-1 has a chemical character more typical of fresh ground water. Analyses suggest that sample WS-4 has a chemical character that could be explained by mixing water similar to WS-1 with water similar to that of samples WS-2 and WS-3. Although samples WS-1 and WS-4 were collected at similar distances from the mountain front, the chemical similarity of WS-4 to WS-2 and WS-3 indicates that the plume of geothermal fluid discharging to the valley-fill depos-

Table 5. Chemical geothermometers applied to analyses of ground-water samples from the Newcastle area. Values are in degrees Celsius. References are [1]Fournier, 1981; [2]Fournier and Truesdell, 1973; [3]Fouillac and Michard, 1981; and [4]Giggenbach, 1988.

GEOTHERMOMETER (Reference)	ESTIMATED RESERVOIR TEMPERATURE (°C) WS-1	WS-2	WS-3	WS-4	WS-5	WS-6
chalcedony [1]	64	97	89	84	51	69
Na-K-Ca [2]	28	99	99	89	32	54
Na-Li [3]	63	115	120	92	32	69
K-Mg [4]	30	110	114	7	30	48

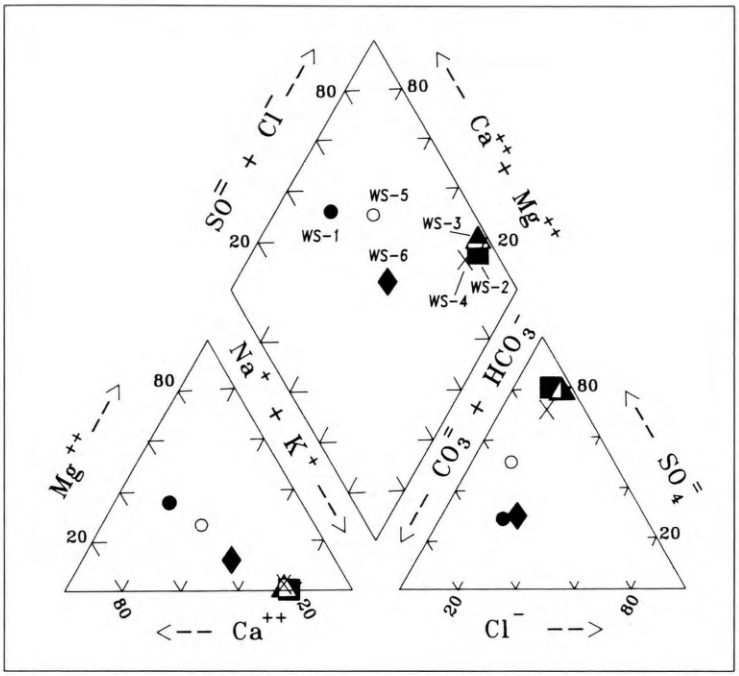

Figure 16. Piper diagram of water analyses obtained for ground-water samples WS-1 through WS-6. Scales are percent of total milliequivalents per liter.

its is moving in a northerly direction rather than radially away from the source. This direction of flow is in general agreement with potentiometric gradients presented by Mower and Sandberg (1982), and also in agreement with the heat-flow contours shown on figure 15. Samples WS-5 and 6 have chemistries that are more difficult to interpret. The relative proportion of cation species (figure 16) suggests that these samples are intermediate between the two groups discussed previously. The relative proportion of anion species of sample WS-6, however, is similar to sample WS-1.

Samples WS-3, WS-2, WS-4, and WS-1 indicate a progression of increasingly mixed fluid. Samples WS-3 and WS-2 appear to contain about 90 percent of the original geothermal fluid, and samples WS-4 and WS-1 appear to contain about 40 percent and 5 percent, respectively, of the original fluid. The distinctive chemical character of sample WS-1 suggests that this sample may be a dilute version of the ground water discharging to the valley-fill deposits, or the sample may be typical of ground-water chemistry found throughout the valley-fill deposits (M.C. Adams, University of Utah Research Institute, personal communication).

Chemical Geothermometry

Geochemical thermometers or geothermometers are empirically derived formulas, primarily based upon the solubility of various mineral phases in aqueous solutions at elevated temperatures. Fournier and others (1974) describe the following assumptions made when applying geothermometers: (1) dissolved constituents are the result of temperature-dependent reactions, (2) an adequate supply of reactants is present in the reservoir, (3) chemical equilibrium between the fluid and rock is established, (4) no re-equilibration takes place after the fluid leaves the reservoir, and (5) reservoir fluid does not mix with other meteoric water.

Table 6. Light-stable isotope analyses of ground-water samples obtained from springs and wells near Newcastle, Utah. Values of δD and $\delta^{18}O$ are expressed in per mil relative to standard mean ocean water (SMOW).

Sample Location	$\delta^{18}O$	δD
Cove Spring	-13.0	-95
Pinto Spring	-13.9,-14.0	-104,-103
Hildebrand Well (WS-2)	-14.2	-107
Troy Hygro Well (WS-3)	-14.0,-14.3	-108
Joel Spring -14.0		-103
Escalante Mine	-13.0	-94
Hamblin Spring	-12.6,-12.4	-91,-92

Table 5 shows the results of chemical geothermometry using the analyses of samples WS-1 through WS-6. In addition, chemical geothermometry

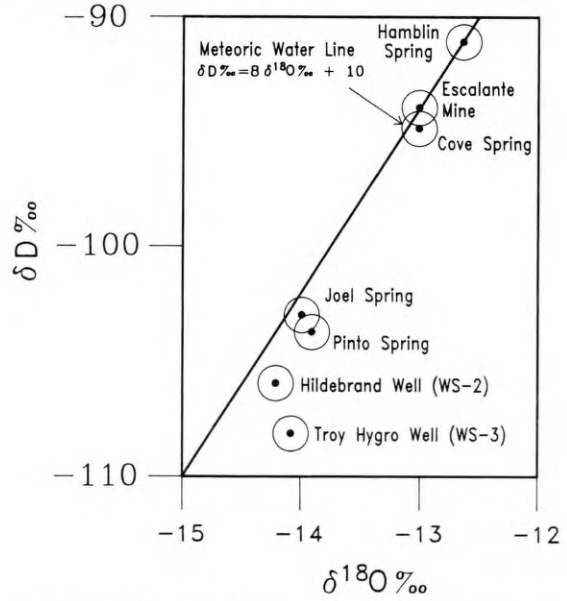

Figure 17. Plot of δD versus $\delta^{18}O$ showing the results of stable isotope analyses of ground-water samples obtained from springs and wells in and near the Newcastle study area. The locations of sampled wells Hildebrand and Troy Hygro are noted on figure 12 as wells WS-2 and WS-3 respectively. Locations of samples from the various springs and from the Escalante mine are indicated on table 6.

was applied to the results of chemical analyses reported by Rush (1983) for a water sample from drill hole NC-10, the Christensen Brothers' discovery well. Estimated equilibration temperatures calculated for analyses of our samples are generally within the range 100 to 120°C (212 to 248°F). Rush's (1983) estimated temperature of 166°C (331°F) for a water sample from drill hole NC-10 (using the Na-K-Ca geothermometer) is considerably higher than geothermometer temperatures obtained from the analyses of our samples. Results computed for WS-1, WS-5, and WS-6 indicate temperatures that fall below the range where geothermometry calculations are applicable.

The maximum computed temperatures from our sample analyses (100°C to 120°C; 212°F to 248°F) approach the maximum recorded temperature of 130°C (266°F) measured at a depth of 106 meters (348 ft) in well CHR-1. This would suggest that the fluid chemistry may reflect conditions more representative of the shallow outflow portion of the hydrothermal system, rather than the deep geothermal reservoir. Samples WS-2 and WS-3 yielded our highest computed temperatures and appear to be mixed the least (up to 90 percent original geothermal fluid) with shallow ground water.

The computed temperature from Rush's (1983) analyses of fluid from well NC-10 (166°C; 331°F using Na-K-Ca), however, suggests a much higher reservoir equilibration temperature. This is somewhat of an enigma, but might be explained by differences of sampling conditions. Our samples WS-2 and WS-3 were taken from wells where only small-duration flows were achieved at the time of sampling. Rush's sample was apparently taken at the end of a 6-hour pump test and would be more likely to reflect actual reservoir conditions in the outflowing geothermal plume.

Stable Isotopes

Analyses of oxygen and hydrogen isotopes were performed by John Bowman of the University of Utah on ground-water samples collected at several wells in the vicinity of Newcastle, and from springs located in the mountains south and east of Newcastle (Blackett and others, 1990, p. 64). These data are tabulated in table 6 and plotted in figure 17. Uncertainty in the analytical results is approximately ± 1 for δD and ± 0.15 for $\delta^{18}O$ values. Where two values are reported for δD or $\delta^{18}O$, each determination was made on different aliquots of the water sample. The average of these data pairs was plotted in figure 17.

Stable isotope data obtained from springs and wells in the Newcastle area span a relatively narrow range of δD and $\delta^{18}O$ values. The results of all analyses lie close to the meteoric water line (MWL) defined by Craig (1961) suggesting that each sample originated as meteoric water with little isotopic fractionation or isotopic exchange with wallrock along the flow path. The meteoric signature of samples WS-2 and WS-3, obtained within the thermal-chemical plume identified previously, suggest that the heated ground water originated as meteoric water that entered the system as recharge from the adjacent highlands, rather than from the loss of volatile constituents from an underlying igneous intrusion. This recharge, deep circulation, heating, and discharge scenario is typical of most basin and range geothermal systems.

The commonly noted correlation between decreasing δD and increasing elevation of ground-water recharge suggests that ground water in the thermal-chemical plume was recharged at higher elevations than ground water sampled at Cove Spring or Hamblin Spring. Review of topographic maps in the Newcastle area indicates that these springs may represent discharge from relatively shallow ground-water flow systems with recharge at higher elevations on the same slope. Relatively deep circulation in a regional-scale flow system with a recharge area that extends to the Pine Valley Mountains 20 kilometers (12 mi) southeast of Newcastle may contribute to the relatively low δD values found in the thermal well samples.

Samples from the thermal wells (WS-2 and WS-3) plus the sample from Pinto Spring plot somewhat to the right of the MWL, suggesting enrichment of ^{18}O. Enrichment in ^{18}O is common for meteoric waters that have experienced temperatures above 40°C (104°F) along their flow paths, and it is also the result of water-rock interaction at elevated temperatures.

ELECTRICAL SURVEYS

In order to better determine the position of the upflowing fluid zone, electrical resistivity and self-potential (SP) geophysical methods were conducted

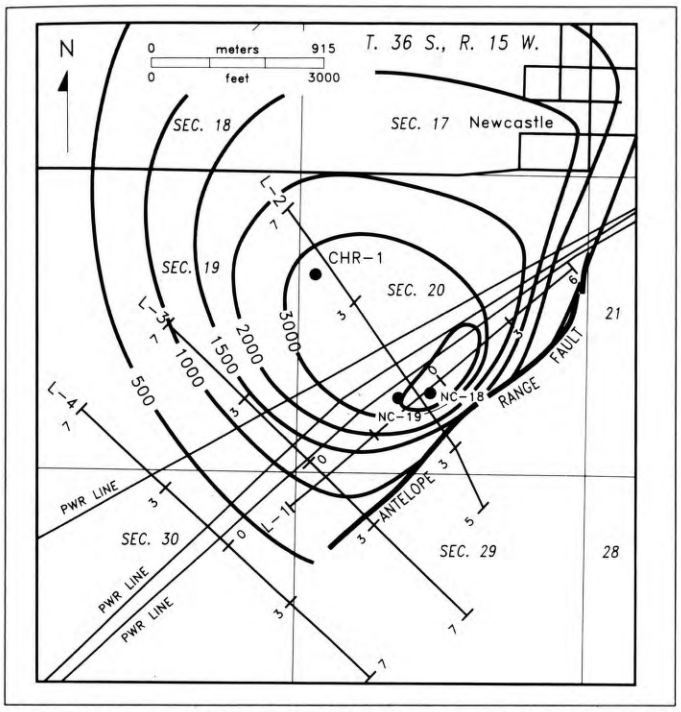

Figure 18. Location of resistivity lines. Note the line locations with respect to the heat-flow anomaly and to temperature-gradient drill holes NC-18, NC-19, and CHR-1. Also note the trace of the Antelope Range fault and the position of high-voltage transmission lines.

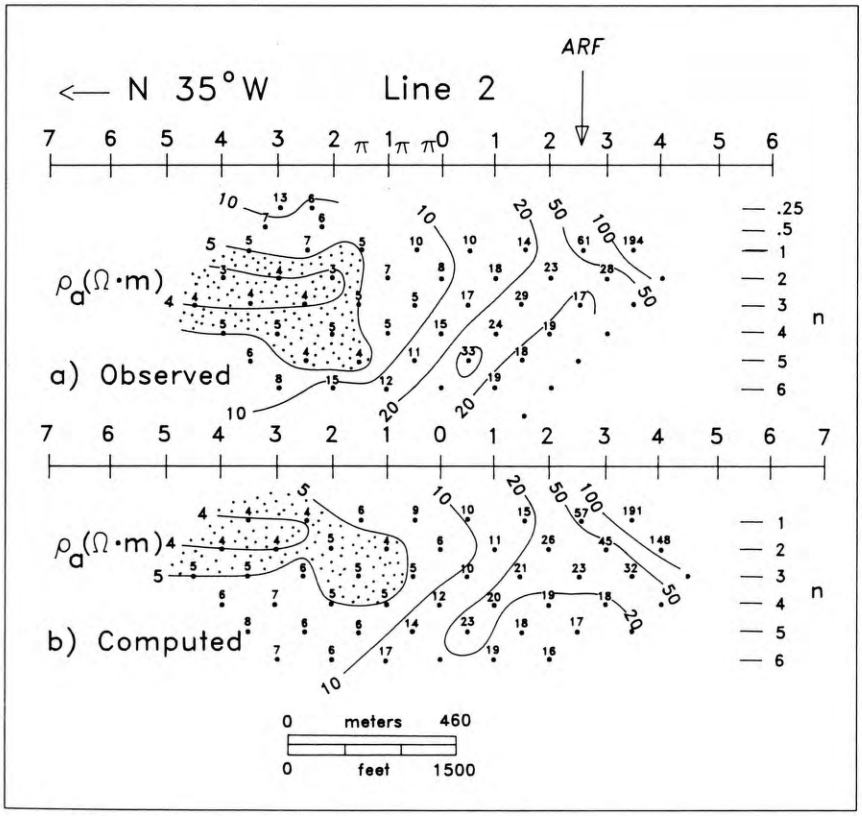

Figure 19. Pseudo sections showing observed apparent resistivity values (a) and computed apparent resistivity values (b) for the model solution shown in figure 21, Newcastle line 2 (after Ross and others, 1990). The symbol π indicates the point where a transmission line crosses the resistivity profile.

(Ross and others, 1990). The goals of these surveys were to accurately locate the upflow zone of the system along an approximate 1,200 meter (4,000 ft) length of the Antelope Range fault, and to map the distribution of the outflow plume.

Resistivity Survey

Because hydrothermal fluid often contains relatively high concentrations of ions in solution, the fluid usually exhibits lower electrical resistivity than the surrounding environment. This makes electrical resistivity methods very useful for mapping fluid-flow patterns in geothermal systems. Although we recognized the potential value of performing resistivity surveys across the Newcastle geothermal area, the survey area was complicated by the presence of many noise-producing, grounded structures. A utility corridor, containing three high-voltage transmission lines that crossed the temperature anomaly from northeast to southwest, restricted the locations available for resistivity survey lines. Other impediments to the resistivity survey included fences, stockyards, and operating irrigation systems located a short distance (300 to 1,500 m) to the northwest. After considering several types of survey options, Ross and others (1990, p. 1,532) chose the dipole-dipole array method, with a dipole length of 152 meters (500 ft) in order to minimize electrical interference from the grounded structures. A dipole length of 152 meters (500 ft) was the best compromise between lateral coverage and vertical resolutions for investigating to a depth of interest of 305 meters (1,000 ft).

In order to minimize electrical disturbances from power transmission lines, Ross (and others 1990, p. 1,533) located four resistivity lines across the thermal area (figure 18). Resistivity line 1 was oriented roughly parallel to the Antelope Range fault and utility corridor, while remaining one dipole length (152 m) or more from the transmission lines. Line 2 was positioned to cross the temperature anomaly, the Antelope

Range fault, and run beneath the power lines in a near-perpendicular orientation. Lines 3 and 4 were oriented similarly to line 2, but were positioned southward from the center of the thermal anomaly. Resistivity lines 2, 3, and 4 were chosen to fall midway between the nearest transmission line towers. Although power line noise was noticeable along line 1, no significant noise was noted on lines 2, 3, and 4. The observed data for line 2 (figure 19a) show very low apparent resistivity values (5Ω·m or less) west of station 1 NW on separations n=1 through n=5, and much higher resistivity values to the southeast. Figure 19b compares the computed apparent resistivity with the numerical-model solution for these data. Computed low-resistivity values often match the data within 1Ω·m, and higher resistivity values match within 10 percent, indicating a good fit to the observed data.

The observed apparent resistivity pattern on line 3 (figure 20) is similar to the pattern seen on line 2, although fewer low-resistivity values were recorded. Line 4 was positioned on a similar orientation and located 610 meters (2,000 ft) southwest of line 3 to determine if the low resistivity values seen on line 2 and line 3 were due to a pervasive low-resistivity clay layer rather than a localized thermal plume. Both near-surface and deep resistivity values observed on line 4 were generally higher than values seen on line 2 and line 3.

Ross and others (1990, p. 1,533) performed numerical modelling studies on the Newcastle resitivity data to provide dimensions and resistivitiy values as solutions to the observed data. The model solutions (figure 21) provide good geometric approximations to the geothermal system. Because the model solutions are non-unique, the intrinsic resistivity values and layer dimensions are based upon geologically reasonable guesses.

The model solutions (figure 21) for line 2 and line 3 show vertical low-resistivity (4 Ω·m) zones rising from depths greater than 300 meters (980 ft). The low-resistivity zones continue to the northwest as horizontal, 100 meter (330 ft) to 150 meter (490 ft) thick layers. Model solutions for line 2 and line 3 show that the near-vertical 4 Ω·m resistivity bodies are about 200 meters (660 ft) down-slope from the mapped trace of the Antelope Range fault. The solution for line 4 shows higher resistivity values for layers in the valley-fill alluvial deposits than the solutions for lines 2 and 3. These higher values on line 4 are possibly more typical of resistivity within the volcanic parent material in the adjacent range.

The modeled solution for line 2 (figure 21) suggests that depth to the top of the thermal system, or outflow plume, ranges between 45 meters (150 ft) on the northwest end of the line and 150 meters (490 ft) near station 1 on the southeast. Similarly, the modeled solution for line 3 indicates that the top of the system, from northwest to southeast, lies at depths between about 45 meters (148 ft) and 90 meters (295 ft). Models for both lines suggest that most of the outflow plume lies at a depth of about 45 m (148 ft), although disagreement between observed and computed resistivity values for so-

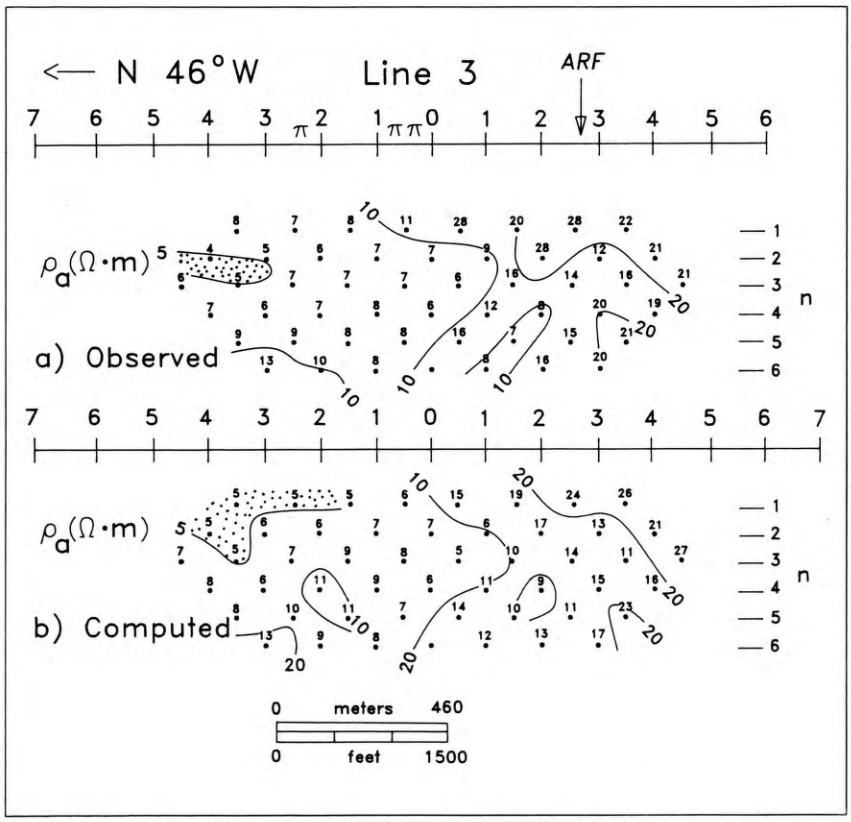

Figure 20. Pseudo sections showing observed apparent resistivity values (a) and computed apparent resistivity values (b) for the model solution shown in figure 21, Newcastle line 3 (after Ross and others, 1990). The symbol π indicates the point where a transmission line crosses the resistivity profile.

lution models suggests the top of the plume may be as deep as 60 meters (197 ft).

Figure 22 is a map of the modeled resistivity distribution for the depth interval 91 to 152 meters (300 to 500 ft) compared to the contoured third separation (n=3) observed resistivity values. The map shows that there is a distinct boundary to the thermal plume on the south and east sides of the thermal area.

Self-Potential Survey

The self-potential (spontaneous-polarization or SP) method for geothermal exploration is relatively simple and inexpensive, and it has detected anomalies related to thermal fluids in many case studies of geothermal systems (Zablocki, 1977; Corwin and Hoover, 1979). In geothermal areas, SP responses can occur as a variety of amplitudes, shapes, multiple anomalies, and can have either positive or negative polarity. Corwin and Hoover (1979) describe the thermoelectric coupling effect and the electrokinetic coupling (streaming potential) effect which give rise to most anomalies associated with geothermal fluid flow.

Ross and others (1990, p. 1534) performed SP surveys at Newcastle to complement earlier electrical resistivity surveys. The Newcastle SP surveys con-

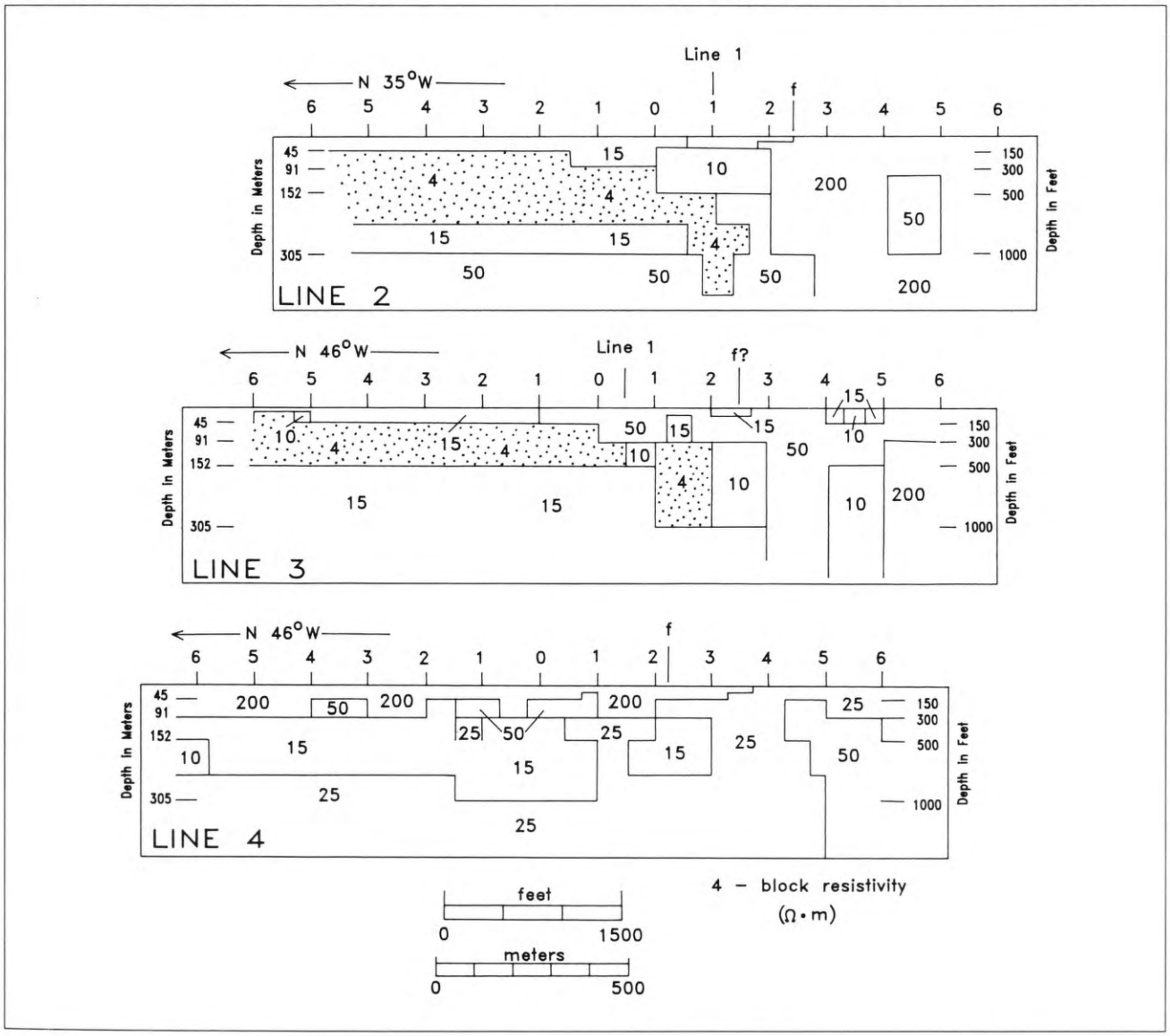

Figure 21. Numerical model solutions for resistivity lines 2, 3, and 4. The low-resistivity bodies (shaded) are interpreted as the fluid conduits and outflow plume (after Ross and others, 1990).

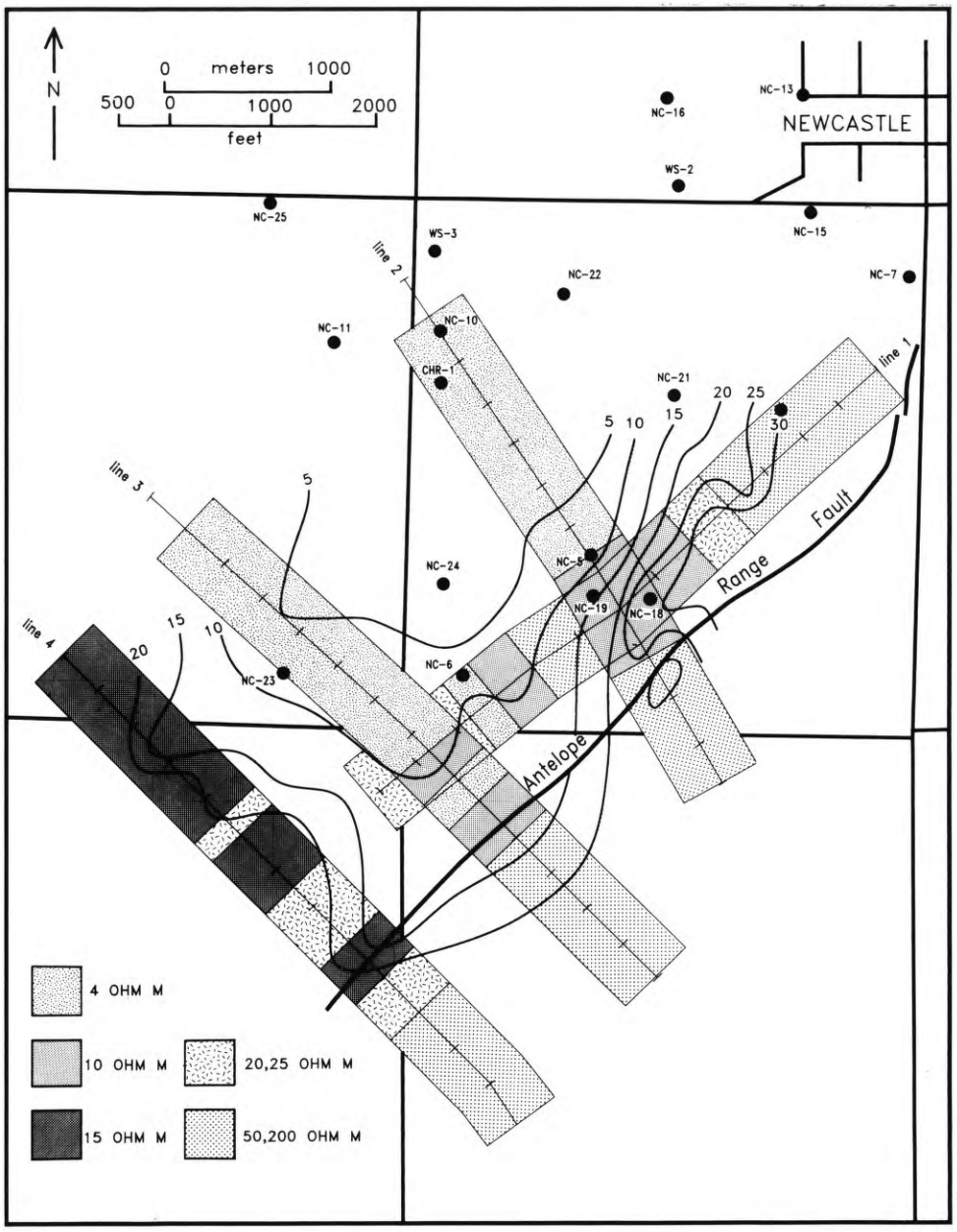

Figure 22. Contoured third separation (n = 3) apparent resistivity and modeled intrinsic resistivity for the depth interval 91-152 meters (300-500 ft) (after Ross and others, 1990).

sisted of eight survey lines as long as 1,220 meters (4,000 ft) with a standard porous pot electrode spacing of 61 meters (200 ft) (figure 23). Noise levels were kept at less than one mV by preparing and watering potholes a number of hours prior to reading. Potential differences were referenced to a low-gradient area, noted as "Reference Base Station" on figure 23, located southwest from the center of the thermal anomaly.

Ross and others (1990) mapped a well-defined 108 mV SP minimum nearly coincident with the center of the observed temperature anomaly (figure 23). The SP minimum is located between drill holes NC-18 and NC-19, where the highest temperature gradients were observed. Close inspection of two perpendicular profiles defining the SP anomaly (lines 2 and 6; figure 24) shows a 2:1 elongation of the anomaly in the direction of the surface trace of the Antelope Range fault.

Ross and others (1990) describe the Newcastle SP anomaly as a short wavelength, 108 mV negative anomaly similar in amplitude, polarity, and wave-

length to the SP anomaly described by Sill and Johng (1979) over the Dome fault at Roosevelt Hot Springs. Based on Sill and Johng's (1979) modelling and its applicability to Newcastle, Ross and others (1990) believe that the Newcastle SP anomaly is likely produced by a point or small three-dimensional source situated at shallow depth. The correlative position and geometry of the SP source along with high near-surface temperatures in shallow drill holes and modeled low-resistivity zones at depth provide strong evidence that the SP source is generated by upflowing thermal fluids within the "throat" of the geothermal system.

CONCLUSIONS

We propose that the center of the upflow zone of thermal fluids at Newcastle lies near holes NC-18 and NC-19 (figure 15 and plate 1). Two independent and spatially coincident data sets which define this center are heat-flow data (figure 15 and self-potential data (figure 23). Two additional data sets lend support to this interpretation. The geologic data indicate possible subsurface inter-section of the Antelope Range fault with older, high-angle faults in the Antelope Range horst block, in coincidence with the center of the heat-flow anomaly (plate 1). Modelling of resistivity data (line 2, figure 21) suggests that a narrow, vertical, low-resistivity zone, probably representing upflowing thermal fluids, coincides with this center. We believe that these four data sets adequately define the center (or throat) of the system and that deeper temperature-gradient drilling and sampling of pristine thermal fluid is warranted. It is possible that "unmixed" thermal fluid, produced from the throat of the system, may be sufficiently hot and have a sufficiently high flow rate to support a small binary power-generating facility.

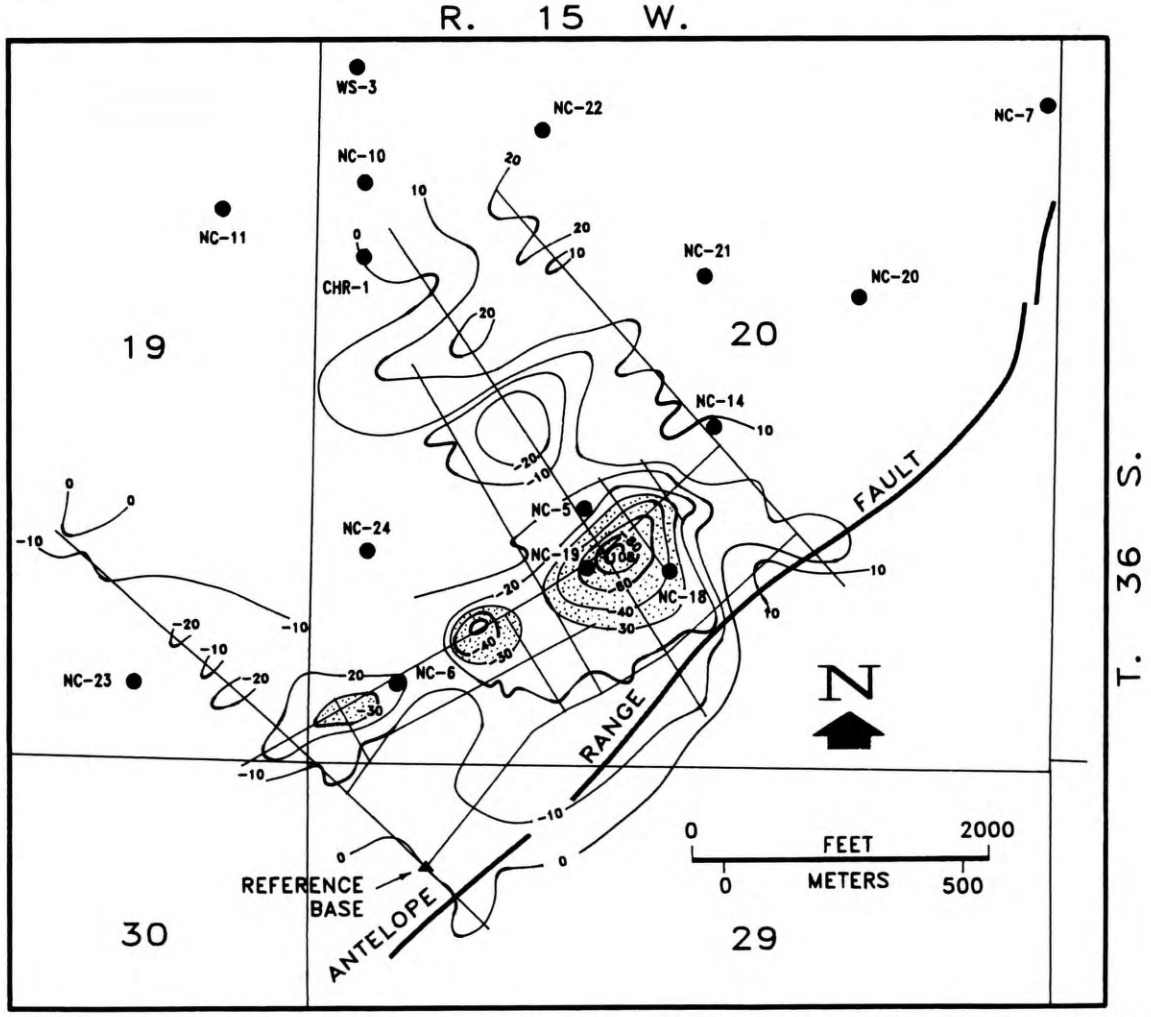

Figure 23. Self-potential map for the Newcastle geothermal area. All values are in mV and are referenced to the base station as noted (after Ross and others, 1990). Stipple pattern denotes areas less than -30 mV.

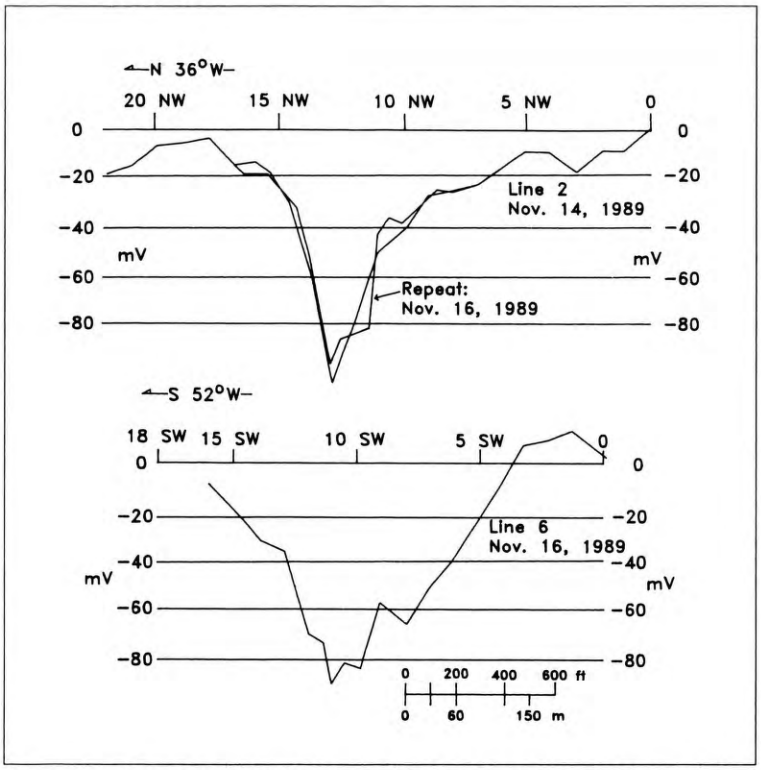

Figure 24. Self-potential profiles for lines 2 (northwest) and 6 (northeast) across the SP minimum. A repeat profile, recorded two days later, on line 2 is also shown (after Ross and others, 1990).

Data from this study support the following model of the Newcastle system, modified from Blackett and others (1990).

1. Thermal fluids originate as meteoric recharge in the Pine Valley Mountains.

2. A complex network of high-angle faults transmits fluids to a depth of several kilometers where the fluid becomes heated by the regional geothermal gradient.

3. The Antelope Range fault taps these fluids and provides an avenue for their ascent. Intersecting high-angle bedrock faults create permeable zones that focus fluid flow to a short segment of the Antelope Range fault.

4. At a depth of about 100 meters (330 ft), upflowing thermal fluids spill into a permeable, Quaternary, valley-fill unit forming the outflow plume.

5. Mixing with cool, near-surface waters occurs in the outflow plume as thermal fluids move in a northerly direction.

Results from this study suggest that the self-potential method is a low-cost, fast method for locating upflow zones of concealed geothermal systems. This technique has been applied in several other parts of the Escalante Desert area with some success (Ross and others, 1990; Ross and others, 1991).

ACKNOWLEDGMENTS

Funding for this work was provided in large part by the U.S. Department of Energy (grant no. DE-FG07-88ID12756). The Utah Geological Survey (UGS) provided support for portions of the geophysical and geological studies as well as contributing UGS personnel time. The Unocal Geothermal Division of the Unocal Corporation provided temperature and other geophysical data from their Christiansen #1 Well.

Gravity data were acquired and reduced by students and teaching assistants of the Department of Geology and Geophysics, University of Utah under the direction of Dr. Charles M. Schlinger. Participants included Susanne Janecke, Joann Hollaway, Rick Hulse, Peter Eick, Jim Hollis, Farhang Namdar, Tim Chisholm, Tony Robertson, and Sean Willett.

Dr. Howard P. Ross of the University of Utah Research Institute, Earth Science Laboratory, provided technical guidance on certain geophysical aspects of the project in addition to directing resistivity and self-potential surveys. Claron Mackelprang, an independent consultant, assisted Dr. Ross with the resistivity data collection and interpretations. Bea Mayes of the UGS also assisted with the resistivity survey.

Dr. David S. Chapman and Dr. Craig B. Forster of the University of Utah Department of Geology and Geophysics directed the heat-flow investigations in the original project and did numerical modelling studies of heat and coupled fluid-flow. B.J. MacPherson, a graduate student at the University of Utah, assisted with the gathering of temperature-gradient and fault-slip data. B.J. was also responsible for determining thermal conductivity from drill cuttings and heat flow values from thermal-gradient data.

Michael C. Adams of the University of Utah Research Institute, Earth Science Laboratory provided helpful suggestions on the interpretation of water chemistry.

We wish to express our thanks to Boyd Christensen, Carroll Tullis, Dan Tullis, Steven Christensen, George Becham, and the other residents of Newcastle for their assistance. We also thank Mary Siders, Peter Rowley, Gary Christenson, and G.L. Galyardt for permission to use unpublished mapping, and Ze'ev Reches for the use of his stress tensor programs. We also express our thanks to Bob Gloyn and Bill Lund of the Utah Geological Survey, Paul Jewell of the University of Utah, Jim Witcher of the Southwest Technology Development Institute, and Jim Moore of the California Energy Company for providing many helpful suggestions to the manuscript.

REFERENCES

Anderson, R.E., 1989, Tectonic evolution of the intermontane system, Basin and Range, Colorado Plateau, and High Lava Plains, *in* Pakiser, L.C., and Mooney, W.D., editors, Geophysical framework of the continental United States: Geological Society of America Memoir 172, p. 163-176.

Anderson, R.E., and Christenson, G.E., 1989, Quaternary faults, folds, and selected volcanic features, Cedar City 1°x 2° quadrangle, Utah: Utah Geological and Mineral Survey Miscellaneous Publication 89-6, 29 p., scale 1:250,000.

Angelier, Jacques, 1979, Determination of the mean principal directions of stress for a given fault population: Technophysics, v. 156, p. T17-T26.

Angelier, Jacques, 1984, Tectonic analysis of fault slip data sets: Journal of Geophysical Research, v. 89, no. B7, p. 5835-5848.

Angelier, Jacques, 1989, From orientation to magnitudes in paleostress determinations using fault slip data: Journal of Structural Geology, v. 11, p. 37-50.

Angelier, Jacques, Colletta, Bernard, and Anderson, R.E., 1985, Neogene paleostress changes in the Basin and Range - a case study at Hoover Dam, Nevada-Arizona: Geological Society of America Bulletin, v. 96, p. 347-361.

Best, M.G., Christiansen, E.H., and Blank, R.H. Jr., 1989, Oligocene caldera complex and calc-alkaline tuffs and lavas of the Indian Peak volcanic field, Nevada and Utah: Geological Society of America Bulletin, v. 101, p. 1076-1090.

Blackett, R.E., Shubat, M.A., Chapman, D.S., Forster, C.B., Schlinger, C.M., and Bishop, C.E., 1990, The Newcastle geothermal system, Iron County, Utah–geology, hydrology, and conceptual model: Utah Geological and Mineral Survey Open-File Report 189, 84 p.

Bodvarsson, Gunnar, 1973, Temperature inversions in geothermal systems: Geoexploration, v. 11, p. 141-149.

Brook, C.A., Mariner, R.H., Mabey, D.R., Swanson, J.R., Guffanti, Marianne, and Muffler, L.J.P., 1979, Hydrothermal convection systems with reservoir temperatures > 90°C, *in* Muffler, L.J.P., editor, Assessment of geothermal resources of the United States - 1978: U.S. Geological Survey Circular 790, 163 p.

Cady, J.W., 1980, Calculation of gravity and magnetic anomalies of finite-length right polygonal prisms: Geophysics, v. 45, p. 1507-1512.

Chapman, D.S., Clement, M.D., and Mase, C.W., 1981, Thermal regime of the Escalante Desert, Utah, with an analysis of the Newcastle geothermal system: Journal of Geophysical Research, v. 86, no. B12, p. 11,735-11,746.

Clement, M.D., 1981, Heat flow and geothermal assessment of the Escalante Desert, part of the Oligocene to Miocene volcanic belt in southwestern Utah: Salt Lake City, University of Utah, Department of Geology and Geophysics, M.S. Thesis, 118 p.

Cook, K.L., Nilsen, T.H., and Lambert, J.F., 1971, Gravity base station network in Utah – 1967: Utah Geological and Mineral Survey Bulletin 92, 57 p.

Corwin, R.F., and Hoover, D.B., 1979, The self-potential method in geothermal exploration: Geophysics, v. 44, p. 226-245.

Craig, H., 1961, Isotopic variations in meteoric water: Science, v. 133, p. 1702-1703.

Denton, E.H., 1976, Helium sniffer test, Newcastle, Utah 10-26 March 1976: U.S. Geological Survey Open-File Report 76-421, 4 p.

Dobrin, M.B., and Savit, C.H., 1988, Introduction to Geophysical Prospecting: McGraw-Hill Book Company, New York City, 867 p.

Eaton, G.P., Wahl, R.R., Prostka, H.J., Mabey, D.R., and Kleinkopf, M.D., 1978, Regional gravity and tectonic patterns - their relationship to late Cenozoic epeirogeny and lateral spreading in the western Cordillera, *in* Smith, R.B. and Eaton, G.P., editors, Cenozoic tectonics and regional geophysics of the western Cordillera: Geological Society of America Memoir 152, p. 51-91.

Fouillac, C., and Michard, G., 1981, Sodium/lithium ratio in water applied to the geothermometry of geothermal waters: Geothermics, v. 10, p. 55-70.

Fournier, R.O., 1981, Application of water geochemistry to geothermal exploration and reservoir engineering, *in* Rybach, L., and Muffler, L.J.P., editors, Geothermal systems - principles and case histories: New York, John Wiley, p. 109-143.

Fournier, R.O., and Truesdell, A.H., 1973, An empirical Na-K-Ca geothermometer for natural waters: Geochimica et Cosmochimica Acta, v. 37, p. 1255-1275.

Fournier, R.O., White, D.E., and Truesdell, A.H., 1974, Geochemical indicators of subsurface temperature – part I, basic assumptions: U.S. Geological Survey Journal of Research, v. 2, no. 3, p. 259-262.

Gephart, J.W., and Forsyth, D.W., 1984, An improved method for determining the regional stress tensor using earthquake focal mechanism data: Application to the San Fernando earthquake sequence: Journal of Geophysical Research, v. 89, no. B11, p. 9305-9320.

Giggenbach, W.F., 1988, Geothermal solute equilibria - derivation of Na-K-Mg-Ca geoindicators: Geochimica et Cosmochimica Acta, v. 52, p. 2749-2765.

Grant, S.K., and Proctor, P.D., 1988, Geology of the Antelope Peak quadrangle, Iron County, Utah: Utah Geological and Mineral Survey Open-File Report 130, 1 pl. 1:24,000, 32 p.

Hem, J.D., 1970, Study and interpretation of the chemical characteristics of natural water: U.S. Geological Survey

Water Supply Paper 1473, 363 p.

Hoover, D.B., and Pierce, H.A., 1987, Audio-magnetotelluric data release for the Newcastle, Utah geothermal area: U.S. Geological Survey Open-File Report 87-69, 6 p.

Klauk, R.H., and Gourley, Chad, 1983, Geothermal assessment of a portion of the Escalante Desert, Utah: Utah Geological and Mineral Survey Special Studies 63, 57 p.

Lachenbruch, A.H., and Sass, J.H., 1978, Models of an extending lithosphere and heat flow in the Basin and Range Province, *in* Smith, R.B., editor, Cenozoic tectonics and regional geophysics of the western Cordillera: Geological Society of America Memoir 152, p. 209-250.

Lachenbruch, A.H., Sorey, M.L., Lewis, R.E., and Sass, J.H., 1976, The near-surface hydrothermal regime of Long Valley caldera: Journal of Geophysical Research, v. 81, no. 5, p. 763-768.

Mabey, D.R., and Budding, K.E., 1987, High-temperature geothermal resources of Utah: Utah Geological and Mineral Survey Bulletin 123, 64 p.

Mardia, K.V., 1972, Statistics of directional data: Academic Press, London, 388 p.

Mase, C.W., Chapman, D.S., and Ward, S.H., 1978, Geophysical study of the Monroe - Red Hill geothermal system: Salt Lake City, University of Utah, Department of Geology and Geophysics Topical Report EY-76-S-07-1601, 89 p.

Mower, R.W., and Sandberg, G.W., 1982, Hydrology of the Beryl-Enterprise area, Escalante Desert, Utah, with emphasis on ground water: State of Utah, Department of Natural Resources, Technical Publication 73, 66 p.

Parasnis, D.S., 1971, Temperature extrapolation to infinite time in geothermal measurements: Geophysical Prospecting, v. 19, p. 612-614.

Pe, Win, 1980, Gravity survey of the Escalante Desert and vicinity in Iron and Washington Counties, Utah: Salt Lake City, University of Utah, Department of Geology and Geophysics, M.S. thesis, 151 p.

Pe, Win, and Cook, K.L., 1980, Gravity survey of the Escalante Desert and vicinity, in Iron and Washington Counties, Utah: Salt Lake City, Earth Science Laboratory, University of Utah Research Institute Report no. DOE/ID/12079-14, 169 p.

Petit, J.P., 1987, Criteria for the sense of movement on fault surfaces in brittle rocks: Journal of Structural Geology, v. 9, no. 5/6, p. 597-608.

Press, W.H., Flannery, B.P., Teukolsky, S.A., and Vetterling, W.T., 1986, Numerical recipes - the art of scientific computing: Cambridge, England, Cambridge University Press, 780 p.

Reches, Ze'ev, 1987, Determination of the tectonic stress tensor from slip along faults that obey the Coulomb yield condition: Tectonics, v. 6, no. 6, p. 849-861.

Ross, H.P., Blackett, R.E., Shubat, M.A., and Mackelprang, C.E., 1990, Delineation of fluid up-flow and out-flow plume with electrical resistivity and self-potential data–Newcastle geothermal area, Utah: Geothermal Resources Council Transactions, v. 14, pt. II, p. 1531-1536.

Ross, H.P., Blackett, R.E., and Shubat, M.A., 1991, Wood Ranch thermal anomaly, Iron County, Utah, self-potential survey and fluid chemistry: Utah Geological Survey Miscellaneous Publication 91-4, 21 p.

Rowley, P.D., and Siders, M.A., 1988, Miocene calderas of the Caliente caldera complex, Nevada-Utah: EOS (Transactions of the American Geophysical Union), v. 69, no. 44, p. 1508.

Rowley, P.D., Steven, T.A., Anderson, J.J., and Cunningham, C.G., 1979, Cenozoic stratigraphic and structural framework of southwestern Utah: U.S. Geological Survey Professional Paper 1149, 22 p.

Rush, F.E., 1977, Subsurface-temperature data for some wells in western Utah: U.S. Geological Survey Open-File Report 77-132, 36 p.

Rush, F.E., 1983, Reconnaissance of the hydrothermal resources of Utah: U.S. Geological Survey Professional Paper 1044-H, p. H1-H49.

Sass, J.H., and Sammel, E.A., 1976, Heat flow data and their relation to observed geothermal phenomena near Klamath Falls, Oregon: Journal of Geophysical Research, v. 81, p. 4863-4868.

Shubat, M.A., and McIntosh, W.S., 1988, Geology and mineral potential of the Antelope Range mining district, Iron County, Utah: Utah Geological and Mineral Survey Bulletin 125, 26 p.

Shubat, M.A., and Siders, M.A., 1988, Geologic map of the Silver Peak quadrangle, Iron County, Utah: Utah Geological and Mineral Survey Map 108, 13 p., scale 1:24,000.

Siders, M.A., 1985, Geologic map of the Beryl Junction quadrangle, Iron County, Utah: Utah Geological and Mineral Survey Map 85, 11 p., scale 1:24,000.

Siders, M.A., 1991, Geologic map of the Mount Escalante quadrangle, Iron County, Utah: Utah Geological and Mineral Survey Map 131, 9 p., scale 1:24,000.

Siders, M.A., Rowley, P.D., Shubat, M.A., Christenson, G.E., and Galyardt, G.L., 1990, Geologic map of the Newcastle quadrangle, Iron County, Utah: U.S. Geological Survey Geologic Quadrangle Map GQ-1690, scale 1:24,000.

Sill, W.R., and Johng, D.S., 1979, Self-potential survey, Roosevelt Hot Springs, Utah: Salt Lake City, University of Utah, Department of Geology and Geophysics Report no. DOE/IDO/78-1701.a.23, 29 p.

Smith, R.B., and Sbar, M.L., 1974, Contemporary tectonics and seismicity of the western United States with emphasis on the Intermountain seismic belt: Geological Society of America Bulletin, v. 85, p. 1205-1218.

Sorey, M.L., Lewis, R.E., and Olmstead, F.H., 1978, The hydrothermal system of Long Valley Caldera, California, U.S. Geological Survey Professional Paper 1044-A, 60 p.

Telford, W.M., Geldart, L.P., Sheriff, R.E., and Keys, D.A., 1976, Applied geophysics: Cambridge, England, Cambridge University Press, 860 p.

Williams, P.L., 1967, Stratigraphy and petrology of the Quichapa Group, southwestern Utah and southeastern Nevada: Seattle, University of Washington, Ph.D. dissertation, 139 p.

Zablocki, C.J., 1977, Self-potential studies in East Puna, Hawaii: Honolulu, Hawaii Institute of Geophysics Report HIG 77-15, 175-195.

Zoback, M.L., Anderson, R.E., and Thompson, G.A., 1981, Cenozoic evolution of the state of stress and style of tectonism of the Basin and Range province of the western United States: London, Philosphical Transactions, Royal Society of London, A 300, p. 407-434.

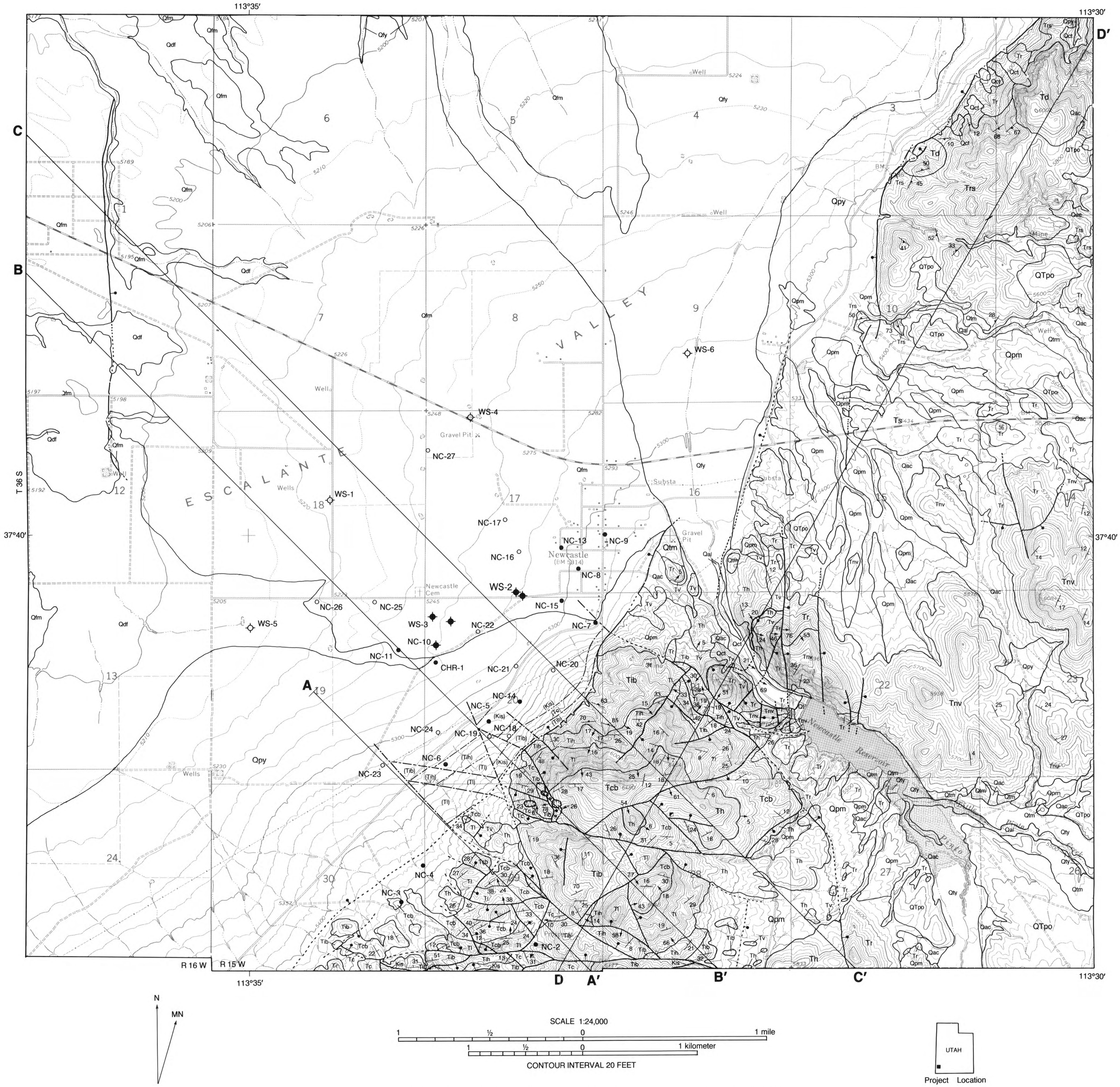

Geology from Siders and others (1989), Geologic map of the Newcastle quadrangle, modified during this study.
Topographic base from U.S. Geological Survey, 1972

Plate 1. Geologic map of the Newcastle geothermal area.

Plate 2. Geologic cross sections, correlation of map units, stratigraphic column, and explanation of symbols for geologic map (plate 1).

Correlation of Map Units

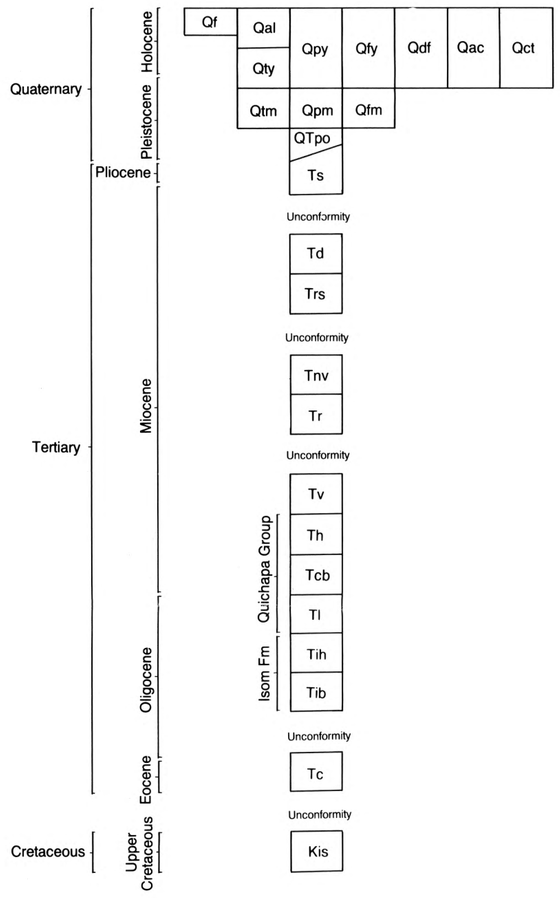

STRATIGRAPHIC COLUMN

SYSTEM	SERIES	FORMATION	MAP SYMBOL	THICKNESS (Feet)	RADIOMETRIC AGE (in Millions of Years)
Tertiary	Miocene	Dacite of Bullion Canyon	Td	?	8.5
		Ryholite of Silver Peak	Trs	?	8.5
		Volcaniclastic Rocks of Newcastle Reservoir	Tnv	300 (980)	>11.6
		Racer Canyon Tuff	Tr	150 (490)	19
		Volcaniclastic Rocks	Tv	40 (130)	
		Harmony Hills Tuff	Th	146 (480)	21
		Bauers Tuff	Tcb	130 (430)	23
	Oligocene	Leach Canyon Tuff	Tl	177 (580)	25
		Hole-in-the-Wall Tuff	Tih	80 (260)	26
		Baldhills Tuff	Tib	335 (1100)	26
	Eocene	Claron	Tc	213 (700)	
Cretaceous	Upper Cretaceous	Iron Springs	Kis	>430 (1400)	

CONTACT

13

Dotted where covered, dash-dot where projected onto footwall of Antelope Range Fault. Arrow and number are direction and dip from three-point solution.

FAULT

35

Dotted where covered, dash-dot where projected onto footwall of Antelope Range Fault. Arrow and number are dip direction and dip from three point solution. Bar and ball on downthrown side. Strike-slip component probable on most faults but no shown.

GRAVITY SLIDE BLOCK

Blocks consist of Harmony Hills Tuff

STRIKE AND DIP OF BEDDING OR ASH-FLOW TUFF LAYERING

23

STRIKE AND DIP OF FLOW LAYERING

32

BRECCIA

Coarse tectonic breccia (megabreccia) lying between fault splays.

LITHOLOGY OF MAP VIEW PROJECTION OF BURIED FOOTWALL OF ANTELOPE RANGE FAULT

(Tih)

PROSPECT

WATER SAMPLE LOCATION

WS-7

GEOTHERMAL WELL

NC-28

TEMPERATURE GRADIENT HOLE DRILLED BY UGS

NC-12

TEMPERATURE GRADIENT HOLE DRILLED BY OTHERS

NC-1

TEMPERATURE GRADIENT HOLE DRILLED BY UGMS